Canadian Mineralogist
Vol. 22, pp. 297-326 (1984)

NATURE AND ORIGIN OF ORTHOPYROXENE MEGACRYSTS FROM THE ST-URBAIN ANORTHOSITE MASSIF, QUEBEC

ROBERT F. DYMEK

Department of Geological Sciences, Harvard University, Cambridge, Massachusetts 02138, U.S.A.

L. PETER GROMET

Department of Geological Sciences, Brown University, Providence, Rhode Island 02912, U.S.A.

ABSTRACT

Al-rich orthopyroxene megacrysts (OPM) in the St-Urbain (Quebec) massif are found in three distinct field associations (leuconorite, anorthosite and anorthositic veinlets); the presence of plagioclase inclusions in OPM and local development of subophitic textures require cocrystallization of OPM and plagioclase. OPM have 0.66 < Mg/(Mg + Fe_T) < 0.72, within the range of other orthopyroxene types in the massif, but contain higher amounts of Ca, Al, Fe^{3+} and Ti. *REE* patterns in OPM and other orthopyroxene are essentially parallel, but OPM are enriched up to a factor of ten. Associated plagioclase-rich materials have An contents, REE patterns, Sr contents and Sr isotopic compositions virtually identical to those found in andesine anorthosite and leuconorite comprising most of the massif. These textural, chemical and isotopic features indicate that the OPM crystallized in the outcrops where they presently reside, from the same anorthositic magma that gave rise to the rocks of the massif as a whole, and that OPM are not relics of remote (upper mantle) crystallization from basalt magma. Narrow plagioclase exsolution lamellae in OPM contain segments occupied by hemoilmenite, suggesting that oxide exsolution is an integral part of the process of their formation. Coupled decomposition of two components originally dissolved in OPM, $R^{2+}{}_2FeTiSi_2Al_2O_{12}$ (FeTi) and $Ca\square Al_2Si_4O_{12}$ (Eskola), explains the calcic composition of the plagioclase lamellae, the development of reverse zoning in essentially all plagioclase contained in and surrounding OPM, and the preponderance of ^{iv}Al over ^{vi}Al in reconstituted (bulk) OPM compositions. Oxidation of pyroxene components to provide silica or an external source of silica is not required. The incorporation of FeTi and Eskola components in original orthopyroxene may be the result of metastable crystallization, where local overstepping of a plagioclase-orthopyroxene cotectic boundary curve has driven the magma to orthopyroxene supersaturation. The localized appearance of OPM supports this. The higher abundances of Ca, Al, Ti, Fe^{3+} and *REE* in OPM compared to other orthopyroxene may be related to the ionic adsorption and retention of these cations onto rapidly growing surfaces of the OPM.

Keywords: orthopyroxene, plagioclase, exsolution, reverse zoning, anorthosite, leuconorite, vacancy, adsorption, rare earths, Sr isotopes, St-Urbain, Quebec.

SOMMAIRE

On trouve de l'orthopyroxène alumineux en mégacristaux (OPM) dans trois associations lithologiques du massif de St-Urbain (Québec): leuconorite, anorthosite et filonnets d'anorthosite. La présence d'inclusions de plagioclase et, localement, de textures subophitiques requiert une syncristallisation des OPM et du plagioclase. Les OPM ont un rapport Mg/(Mg + Fe_T) compris entre 0.66 et 0.72, donc dans l'intervalle des autres types d'orthopyroxène du massif, mais leur teneur en Ca, Al, Fe^{3+} et Ti est nettement plus élevée. Les proportions de terres rares dans les OPM et autres types d'orthopyroxène définissent des lignées parallèles mais décalées par un facteur de 10 en faveur des OPM. Les roches associées enrichies en plagioclase ont des teneurs en An, terres rares et Sr et une composition isotopique du Sr pratiquement identiques à celles de l'anorthosite à andésine et de la leuconorite qui constituent la majeure partie du massif. Ces caractères texturaux, chimiques et isotopiques font penser que les OPM ont cristallisé *in situ*, à partir du magma anorthositique d'où sont issues les roches du massif. De ce fait, les OPM ne seraient pas reliques d'une cristallisation profonde (dans le manteau supérieur) d'un magma basaltique. L'hémoilménite se présente dans d'étroites lamelles d'exsolution de plagioclase dans les OPM. Ceci fait penser que l'exsolution d'un oxyde participe au processus de formation de ces lamelles. Une déstabilisation simultanée des composants $R^{2+}{}_2FeTiSi_2Al_2O_{12}$ (pôle FeTi) et $Ca\square Al_2Si_4O_{12}$ (pôle d'Eskola) originellement dissous dans les OPM expliquerait la composition calcique des lamelles de plagioclase, le développement d'une zonation inverse dans pratiquement tous les grains de plagioclase inclus dans les OPM ou entourant ceux-ci, et la prédominance de ^{iv}Al sur ^{vi}Al dans les compositions globales reconstituées des mégacristaux. Ni l'oxydation de composants du pyroxène ni l'existence d'une source externe de silice n'est requise. L'incorporation du composant dit FeTi et de celui d'Eskola dans l'orthopyroxène originel pourrait résulter d'une cristallisation métastable, due à l'enjambement local de la courbe cotectique entre plagioclase et orthopyroxène, causant la sursaturation du bain en orthopyroxène. La distribution localisée des OPM étaye cette façon de voir. La surabondance de Ca, Al, Ti et terres rares dans les OPM comparés à d'autres pyroxènes pourrait refléter l'adsorption de cations et leur incorporation sur les faces à croissance rapide des mégacristaux d'orthopyroxène.

(Traduit par la Rédaction)

Mots-clés: orthopyroxène, plagioclase, exsolution, zonation inverse, anorthosite, leuconorite, lacune, adsorption, terres rares, isotopes de strontium, St-Urbain, Québec.

INTRODUCTION

Orthopyroxene megacrysts (OPM), which locally reach dimensions in excess of 50 cm, constitute a rare but ubiquitous feature of many massif-type anorthosites. In a recent summary of several occurrences, Emslie (1975) distinguished two varieties: type-I OPM, which are typically Al-rich (~3–9 wt. % Al_2O_3 and contain oriented plagioclase lamellae of probable exsolution origin, and type-II OPM, which lack these features and are found in pegmatoidal masses. Emslie postulated that type-I OPM formed at a very early stage in the magmatic development of anorthositic complexes, possibly at great depth prior to the crystallization of plagioclase. Hence, they could represent "xenocrysts" that were physically transported from their site of formation and are only indirectly related to their present host-rocks. Viewed this way, such OPM may preserve heretofore unrecognized chemical characteristics relevant to anorthosite petrogenesis. In particular, these OPM could conceivably represent cryptic evidence for the "missing" ultramafic cumulate rocks necessary to support a parental basaltic magma for anorthosites (*cf.* Bowen 1917).

Morse (1975), on the other hand, suggested that OPM in layered anorthositic rocks from the Nain complex, Labrador, which resemble type-I OPM of Emslie, formed largely *in situ* as a result of unusual conditions of crystallization. He based this conclusion on the observation that OPM are found at several different stratigraphic levels in the same intrusive unit, as well as on textural features and some chemical data. Bohlen & Essene (1978) described a

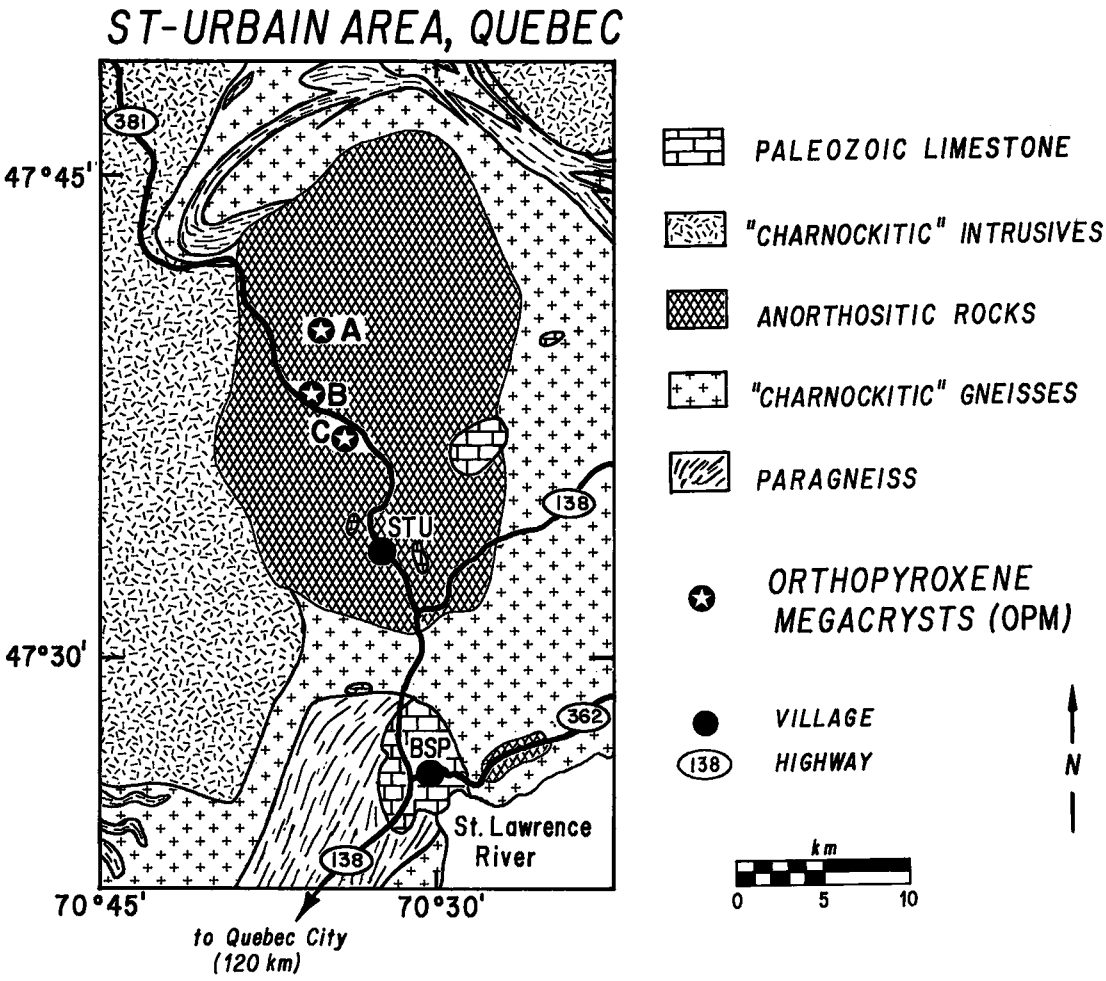

FIG. 1. Simplified geological map of the St-Urbain area, Quebec (adapted from Rondot 1979). Localities of the three OPM occurrences described in the text are shown. STU St-Urbain, BSP Baie St-Paul.

type-I OPM from the Adirondack massif, and favored high temperatures of crystallization as the primary cause for elevated contents of aluminum.

In our ongoing investigation of the St-Urbain anorthosite massif, we have identified OPM-bearing rocks in three distinct associations: (A) in thin (< 10 cm) andesine anorthosite veinlets, (B) in subophitic leuconorite, and (C) in very coarse-grained, massive anorthosite–leuconorite. All OPM studied by us are aluminous, with plagioclase lamellae, and appear similar in most respects to previously described type-I occurrences.

In this report, we summarize the petrography, mineral chemistry, Sr-isotope and rare-earth-element geochemistry of OPM from these three field associations. The majority of our data and observations are consistent with a "local" origin for OPM at St-Urbain (*cf.* Gromet & Dymek 1981a). However, we have observed an extraordinary degree of textural complexity that belies the apparent simplicity implicit in previous discussions of this subject.

Geological Setting

The St-Urbain massif is located ~120 km northeast of Quebec City, and is situated within the central high-grade granulite terrane of the Grenville structural province. An age of crystallization for the massif has yet to be determined, although it is presumably in the range 1000–1400 Ma, based on its occurrence in the "anorthosite belt" of northeastern North America.

As illustrated in Figure 1, the St-Urbain massif is a relatively small, oval body (~ 15 × 30 km). It is composed almost exclusively of anorthositic rocks, dominantly andesine anorthosite of several textural types, with minor leuconorite and a few small deposits of Fe–Ti oxides (Mawdsley 1927, Roy *et al.* 1972, Rondot 1979). Available petrological and geochemical data indicate a comagmatic relationship for these lithologies (Gromet & Dymek 1981b). In addition, as much as 15% of the massif is underlain by relatively older labradorite anorthosite that is petrologically, geochemically and isotopically distinct from, and apparently not directly related to, the andesine anorthosite (Dymek 1980, Gromet & Dymek 1980). OPM are recognized only within those portions of the massif with plagioclase of andesine composition.

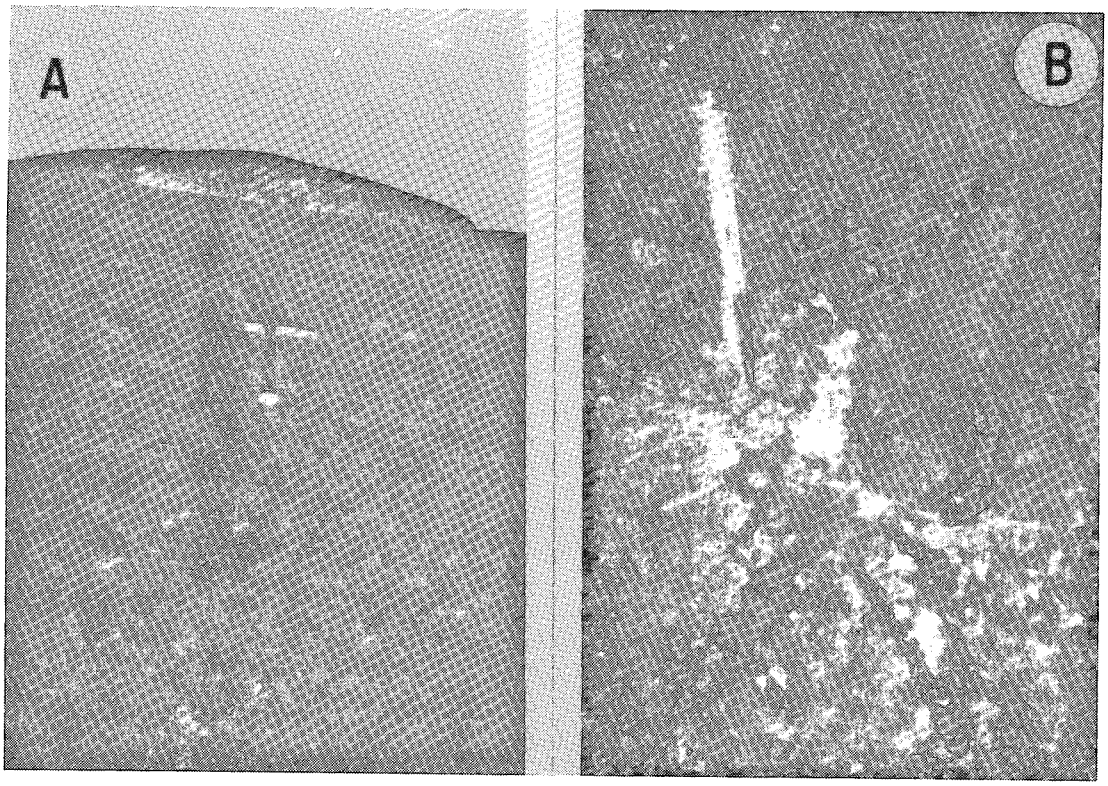

FIG. 2. (A) Thin dyke of andesine anorthosite cutting labradorite anorthosite. (B) OPM in anorthositic vein. Both are from Mont du Lac-des-Cygnes, locality A in Figure 1.

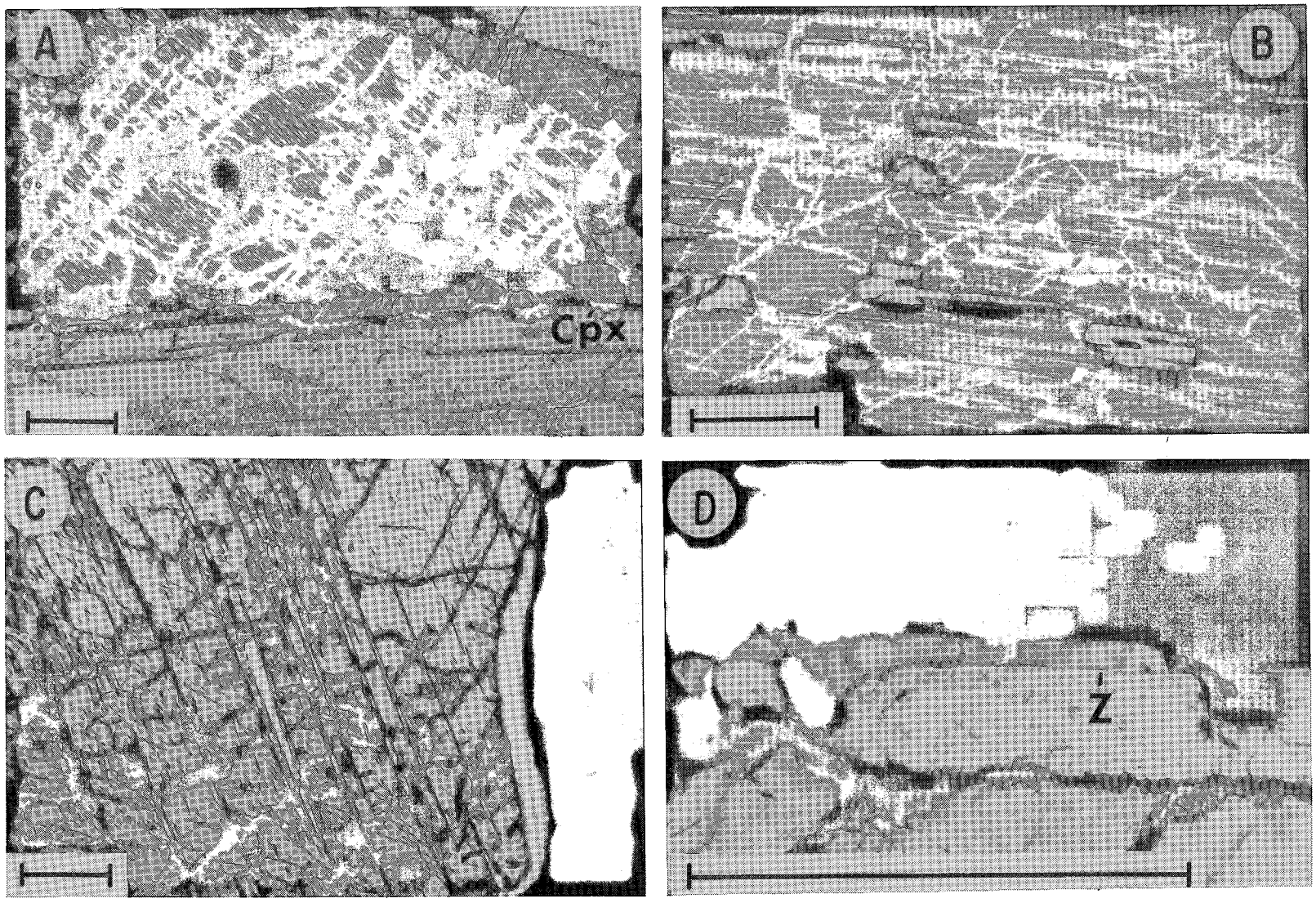
A
Cpx
B
C
D
Z

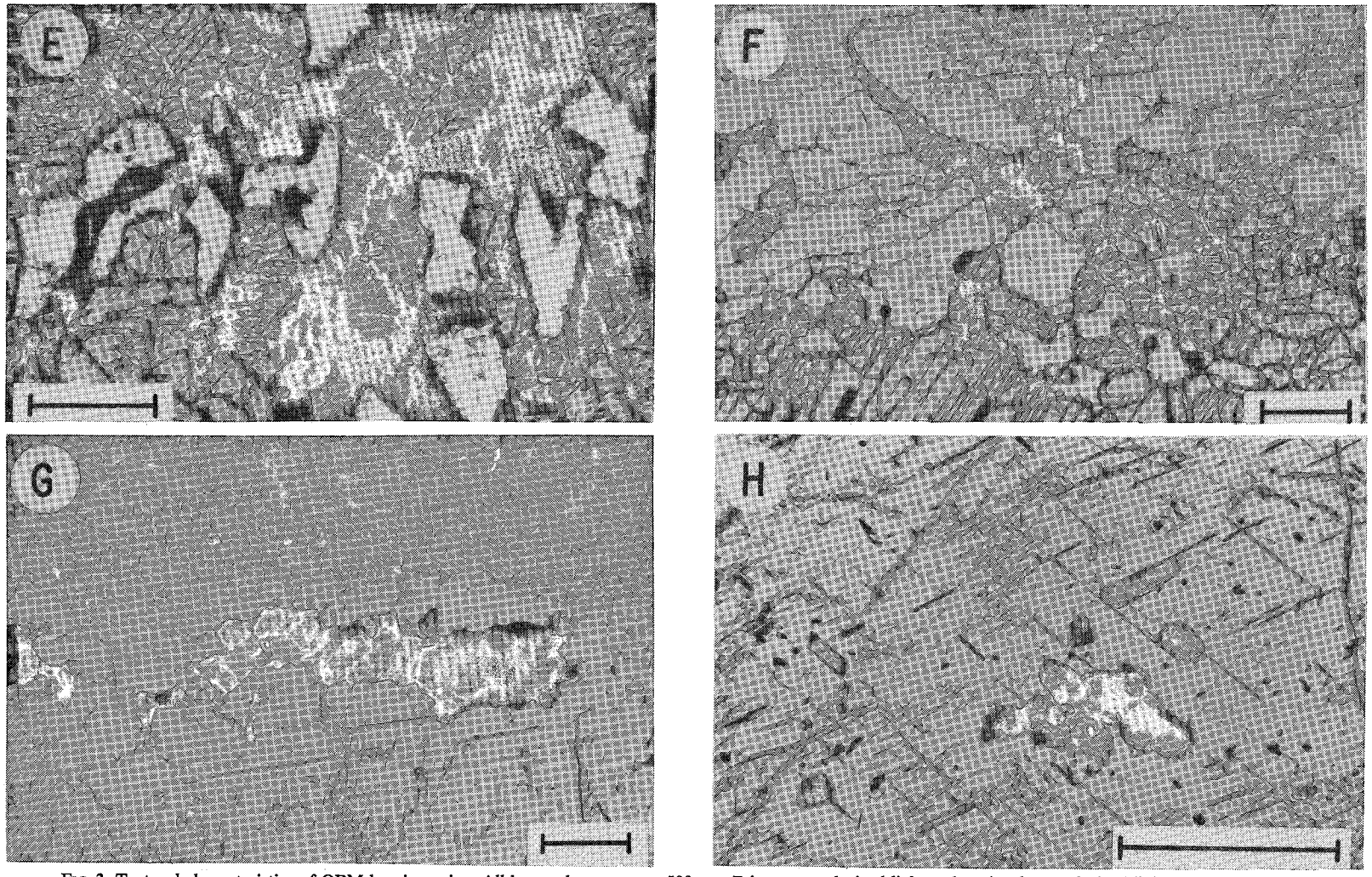

FIG. 3. Textural characteristics of OPM-bearing veins. All bar scales represent 500 μm; B in cross-polarized light, others in plane-polarized light; sample numbers indicated. (A) Clear clinopyroxene "rim" surrounding OPM (MLC 21-3). (B) Thin lamellae of clinopyroxene, and patchy clinopyroxene domains in OPM (MLC 21-8). (C) OPM containing thin lamella of plagioclase; note elongate plagioclase at OPM–oxide boundary (MLC 21-9). (D) Closeup of OPM–oxide boundary illustrated in (C); note the irregular form of the zircon (*Z*) separating plagioclase from oxide here (MLC 21-9). (E) Elliptical inclusions of plagioclase in OPM (MLC 21-9). (F) Plagioclase–orthopyroxene intergrowth at OPM margin; note presence of apatite (*AP*) (MLC 21-8). (G) Anhedral clinopyroxene interstitial to coarse antiperthitic plagioclase (MLC 21-3). (H) Blocky inclusions of clinopyroxene within antiperthitic plagioclase (MLC 21-3).

In general, the massif lacks penetrative deformation, corona structures, and other evidence for significant postmagmatic modification, although the border zones (approximately 1 km wide) are commonly foliated, a feature that is probably related to emplacement of the anorthosite to its present level in the crust (Roy *et al.* 1972, *cf.* Martignole & Schrijver 1970). The country rock consists predominantly of pyroxene-bearing granitoid intrusive bodies and gneisses ("charnockite"), although complexly deformed paragneisses bound the massif along part of its northern margin (Fig. 1). At one locality near the northwestern corner of the massif, a thin (100 m or less) unit of apatite- and oxide-rich norite (Powell *et al.* 1982) separates anorthosite from the "charnockitic" intrusive rocks.

OPM in Anorthositic Veins and Dykes

Field characteristics

At several localities in the St-Urbain massif, dykes of andesine anorthosite intrude a wall rock of labradorite anorthosite (Mawdsley 1927, Dymek 1980). On Mont du Lac-des-Cygnes (MLC; locality A in Fig. 1), these cross-cutting relationships are exceptionally well developed (Fig. 2A). Here, the anorthositic dykes are typically porphyritic, being composed of 10–75% blue-black plagioclase megacrysts (~3–30 cm) set in a finer-grained matrix of pink to grey plagioclase, although narrow dykes tend to lack conspicuous plagioclase megacrysts. Associated with the dykes are numerous thin (<10 cm wide) anorthositic veins that range from straight-walled to highly irregular, and locally occur in "swarms" with an anastomosing habit. The veins appear related to the anorthositic dykes and, in a few cases, apophyses from larger dykes clearly demonstrate such a transition.

In general, the veins are composed of subequigranular, millimetre-sized pinkish brown plagioclase, and are host to rare OPM, which range from 2 to 5 cm across. As illustrated in Figure 2B, individual OPM may be nearly as large as the width of the vein in which they occur. This feature makes it highly unlikely that OPM from this association were transported great distances, and suggests *in situ* formation. However, we have not observed OPM that crystallized inward directly from vein walls. In a few cases, OPM occur in Fe–Ti oxide-rich segregations that are up to 20 cm across.

The anorthositic dykes and veins are similar petrographically, and consist almost entirely of antiperthitic plagioclase (~98%) with mean compositions in the range An_{33} to An_{45}. Minor amounts of interstitial quartz – plagioclase myrmekite, clinopyroxene and hemoilmenite typically are present, along with traces of biotite and rare sulfide and apatite. Orthopyroxene is exceedingly rare in anorthositic dykes and veins, and most samples contain none. The most common occurrence of orthopyroxene in andesine anorthosite on MLC is, in fact, as OPM in the veins, although it is not very abundant in this association either.

Petrography and mineral chemistry

Three samples exhibiting a range of textures were studied in detail and are described below. Two represent OPM in anorthositic veins, and the third an OPM in an oxide-rich segregation. The form of the outcrops necessitated sampling by drilling. Hence, only a small amount of material was available, and no attempt was made to separate individual OPM for "bulk" chemical analysis or for trace-element studies. Moreover, the petrographic complexities of each sample are such that this would have been a futile effort.

The OPM are typically "massive" objects, with a somewhat mottled appearance owing to an abundance of thin (micrometre-sized) exsolved plates of oxide (hemoilmenite) and localized alteration along fractures (Fig. 3A). Rare micrometre-sized exsolution lamellae of clinopyroxene are found in all OPM, and in sample MLC 21–8, the OPM contains patchy clinopyroxene "domains" (up to 50 μm across) that are elongate parallel to the orientation of the clinopyroxene lamellae and appear to be of exsolution origin (Fig. 3B).

The OPM contain scattered lamellae of plagioclase up to 100 μm wide, oriented parallel to (100) of the host (Fig. 3C). These lamellae may display abundant albite twinning in which the (010) composition plane deviates 30–90° from the direction of elongation of the lamellae. In general, the lamellae in these samples are stubby with tapered ends; they are all less than ~3 mm in length, and do not extend to the edge of the OPM. Oxide granules comprise portions of many lamellae, and in a few cases are localized at the ends of an individual lamella.

In addition to their common occurrence as lamellae, plagioclase and oxide are also present as isolated, anhedral grains (up to 250 and 1000 μm, respectively) that have the textural characteristics of inclusions. In sample MLC 21–9, one OPM has a "sieve texture" marked by crescent-shaped inclusions of plagioclase and elliptical inclusions of hemoilmenite (Fig. 3E). In sample MLC 21–8, a complex plagioclase + oxide + clinopyroxene + biotite + apatite inclusion takes the form of a "microvein" (~100 μm wide).

In general, the central portions of OPM ("cores") are similar in the samples studied, but the outer portions ("rims") are remarkably variable. In sample MLC 21–3, an OPM is surrounded by a layer of clinopyroxene up to 500 μm thick (Fig. 3A). It is possible that this clinopyroxene formed by grain-boundary exsolution from a primary pigeonite, but

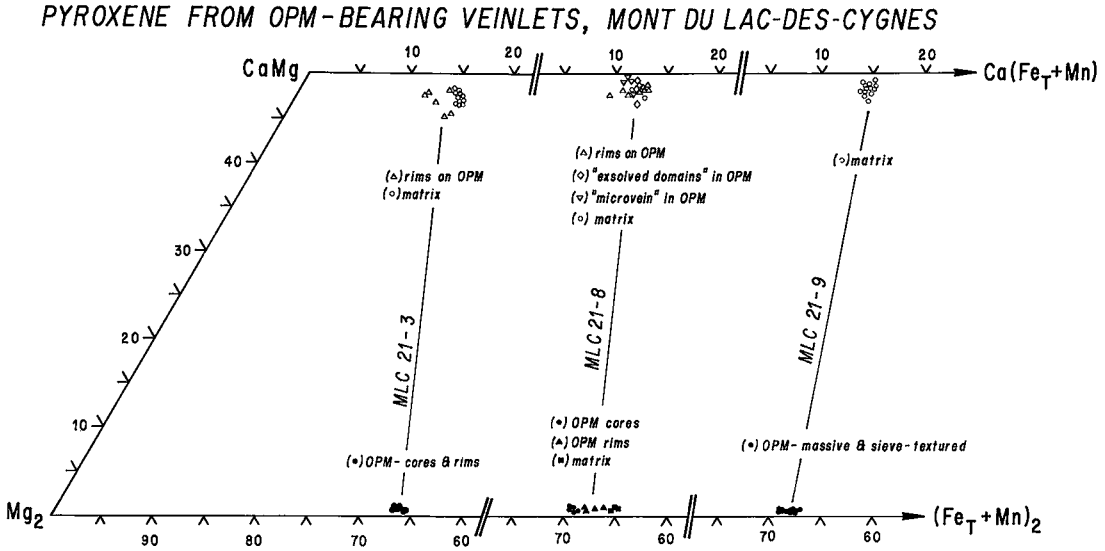

FIG. 4. Compositions of pyroxene from OPM-bearing veins; see text for description of types of pyroxene textures.

the textures provide no definitive criteria by which this hypothesis could be tested.

In MLC 21-8, the massive OPM core is surrounded by an optically continuous rim of irregularly shaped granular orthopyroxene intergrown with clinopyroxene, plagioclase, biotite, oxide and apatite (Fig. 3F). In MLC 21-9, a thin layer (< 50 μm) of plagioclase occurs where the OPM abuts against coarse hemoilmenite (Fig. 3C); in addition, elongated grains of zircon (~10 × 100 μm) are strung out along this boundary at the oxide-plagioclase interface (Fig. 3D). Elsewhere in this sample, biotite aggregates (up to 5 mm across) are present; in one case, biotite is intergrown with and apparently replaces the OPM. In another area, veinlike masses of plagioclase + pyrite + magnetite + hemoilmenite + biotite + apatite separate adjacent OPM. The complexity of these textures and the association of OPM with a wide range of accessory phases are inconsistent with an origin for the OPM during an early isolated stage of crystallization.

Pyroxene compositions are illustrated in Figure 4; representative compositions are listed in Table 1. In each sample, the OPM are fairly homogeneous, with a limited range of composition (~En_{65-69}); the rim may be slightly more Fe-rich than the core. Al_2O_3 contents range from ~ 2.5 to 3.5 wt. % in the core, with values as low as ~ 1.5 wt. % found in the rim. In addition, Al_2O_3 decreases slightly toward lamellae and inclusions of plagioclase. The small grains of orthopyroxene from the matrix of sample MLC 21-8 have a composition ~En_{64}, with ~1.0 wt. % Al_2O_3. In general, there is a slight progressive compositional change from OPM core to OPM rim to matrix grains.

The typical occurrence of clinopyroxene in these samples is as anhedral grains (~25-500 μm across) along plagioclase grain boundaries in the matrix (Fig. 3G), and as blocky inclusions (<50 μm) in matrix plagioclase (Fig. 3H), where they may form granular aggregates with oxide. The various clinopyroxene types show little variation in composition within a given sample (~$Ca_{48}Mg_{36}Fe_{16}$ to ~$Ca_{48}Mg_{40}Fe_{12}$). However, clinopyroxene that surrounds OPM in MLC 21-3 (~$Ca_{46}Mg_{41}Fe_{13}$) is distinct from matrix. In MLC 21-8, a distinction between matrix clinopyroxene and that associated with the OPM is not apparent, although clinopyroxene grains in the "exsolved domains" are the most aluminous ones present. In general, clinopyroxene from these samples is fairly Na-, Al- and Ti-rich (up to 0.8 wt. % Na_2O, 4.5 wt. % Al_2O_3 and 1.1 wt. % TiO_2), and resembles clinopyroxene from the anorthositic dykes (Dymek 1980).

Plagioclase in the matrix comprises polygonal to irregularly shaped grains ranging from <1 to ~25 mm across. They are typically strongly antiperthitic (up to ~5 vol. % exsolved K-feldspar), and contain numerous submicrometre-sized exsolved (?) needles of oxide. As illustrated in Figure 5, matrix plagioclase represents the most sodic type and is fairly homogeneous, with measured compositions spanning ~5 mole % An (MLC 21-3, An_{36-42}; MLC 21-8, An_{42-47}; MLC 21-9, An_{37-43}).

Plagioclase along *every* grain boundary with pyroxene is characterized by a narrow region (<50 μm wide) in which exsolved K-feldspar and oxides are absent, and compositions change continuously and unidirectionally from that of the nearby matrix up to ~An_{60} as pyroxene is approached. Such

TABLE 1. COMPOSITION OF PYROXENE FROM OPM-BEARING VEINLETS, MONT DU LAC-DES-CYGNES*

	1.	2.	3.	4.	5.	6.	7.	8.	9.	10.	11.	12.	13.	14.	15.	16.	17.
Na_2O	0.02	0.00	0.66	0.80	0.63	0.00	0.01	0.01	0.52	0.54	0.44	0.48	0.02	0.01	0.03	0.65	0.50
MgO	23.17	23.40	12.99	12.05	12.50	24.18	24.26	23.14	13.18	13.35	13.98	13.14	24.13	24.05	23.82	12.25	12.41
Al_2O_3	2.00	1.61	3.80	4.13	2.61	2.74	1.67	1.07	4.37	4.72	3.39	2.75	3.52	2.18	3.01	3.70	2.80
SiO_2	51.81	52.33	50.96	49.81	50.88	52.57	53.18	52.98	50.16	50.04	51.29	51.84	52.14	53.14	52.79	50.82	51.39
CaO	0.37	0.46	21.89	22.05	22.60	0.48	0.38	0.45	22.83	23.47	22.11	23.21	0.33	0.39	0.36	22.79	23.01
TiO_2	0.11	0.13	0.57	1.04	0.33	0.13	0.05	0.09	0.86	0.74	0.48	0.46	0.11	0.13	0.14	0.95	0.27
Cr_2O_3	0.02	0.03	0.01	0.00	0.00	0.01	0.04	0.04	0.02	0.02	0.04	0.01	0.03	0.02	0.03	0.00	0.00
MnO	0.47	0.46	0.19	0.21	0.21	0.32	0.39	0.43	0.12	0.11	0.12	0.15	0.46	0.55	0.46	0.21	0.18
FeO_T	21.21	20.57	9.22	9.54	9.55	19.07	19.93	21.43	7.34	6.98	6.98	7.65	19.21	19.90	19.60	9.12	9.39
Total	99.18	98.99	100.29	99.63	99.31	99.50	99.91	99.64	99.40	99.97	99.83	99.65	100.25	100.37	100.24	100.49	99.95
FORMULA PROPORTIONS BASED ON 4 CATIONS AND 6 OXYGEN ATOMS																	
Si	1.930	1.951	1.890	1.866	1.912	1.935	1.955	1.969	1.869	1.850	1.898	1.932	1.915	1.946	1.934	1.889	1.921
Al	0.070	0.049	0.110	0.134	0.088	0.065	0.045	0.031	0.131	0.150	0.102	0.068	0.085	0.054	0.066	0.111	0.079
Al	0.018	0.021	0.056	0.049	0.028	0.054	0.027	0.016	0.061	0.056	0.046	0.052	0.067	0.040	0.064	0.051	0.044
Cr	0.001	0.001	0.000	0.000	0.000	0.000	0.001	0.001	0.001	0.001	0.001	0.000	0.001	0.001	0.001	0.000	0.000
Fe 3+	0.047	0.020	0.069	0.084	0.087	0.004	0.014	0.009	0.058	0.091	0.059	0.024	0.012	0.006	0.000	0.055	0.056
Ti	0.003	0.004	0.016	0.029	0.009	0.004	0.001	0.003	0.024	0.021	0.013	0.013	0.003	0.004	0.004	0.027	0.008
Mg	1.287	1.300	0.718	0.673	0.700	1.327	1.329	1.282	0.732	0.736	0.771	0.730	1.314	1.314	1.301	0.679	0.691
Mn	0.015	0.015	0.006	0.007	0.007	0.010	0.012	0.014	0.004	0.003	0.004	0.005	0.014	0.017	0.014	0.007	0.006
Fe 2+	0.614	0.621	0.217	0.215	0.213	0.583	0.613	0.657	0.171	0.124	0.157	0.214	0.575	0.603	0.600	0.229	0.237
Ca	0.015	0.018	0.856	0.885	0.910	0.019	0.015	0.018	0.912	0.930	0.916	0.927	0.013	0.015	0.014	0.907	0.921
Na	0.001	0.000	0.052	0.058	0.046	0.000	0.001	0.001	0.038	0.039	0.032	0.035	0.001	0.001	0.001	0.047	0.037

MLC 21-3B
1. OPM core
2. OPM rim
3. Cpx "rim" on OPM
4. Interstitial cpx
5. Cpx inclusion in plag

MLC 21-8
6. OPM core
7. OPM rim
8. Matrix opx
9. Exsolved cpx in OPM
10. Cpx from "veinlet" in OPM
11. Cpx at OPM border
12. Interstitial cpx

MLC 21-9
13. Core of "massive" OPM
14. Rim of "massive" OPM
15. Core of "sieve-textured" OPM
16. Interstitial cpx
17. Cpx inclusion in plag

**Based on microprobe analysis*

"reverse zoning" occurs against OPM, matrix orthopyroxene, interstitial clinopyroxene and clinopyroxene inclusions; but only compositions associated with orthopyroxene are illustrated in Figure 5 (others are similar). An intriguing aspect of the reverse zoning is its presence along boundaries with apatite near an OPM margin in sample MLC 21-8.

Compositions of plagioclase lamellae are highly variable both within and among samples, with the total range of measured values being An_{50} to An_{77}. The lamellae are more calcic than matrix plagioclase from the corresponding samples, and in addition show slight reverse zoning. We have not been able to establish whether there is a correlation between size of the OPM and composition of the lamellae or between location of the lamellae and their composition.

Plagioclase from inclusions and "microveins" in OPM is also more calcic than matrix plagioclase, and reversely zoned. Similarly, plagioclase separating OPM from oxide in sample MLC 21-9 (*cf.* Fig. 3C) has a measured composition An_{58-68}, and is reversely zoned.

OPM in Leuconorite

Field characteristics

A heterogeneous suite of leuconorites (exposed in a gently sloping outcrop along the side of Highway 381; locality B in Fig. 1) consists of 60–90 % pinkish brown plagioclase, 40–10 % orthopyroxene, minor hemoilmenite and traces of biotite. Wherever orthopyroxene crystals exceed ~1 cm in size, plagioclase lamellae are observed to occur.

Although there is a wide variation in texture and grain size, two varieties predominate. One is "medium-grained" and typically equigranular (Fig. 6A); the other is "coarse-grained" but otherwise appears equivalent. In the latter, plagioclase commonly is tabular, and a subophitic texture is present where orthopyroxene fills interstices between laths (Fig. 6B). Individual laths of plagioclase range up to 5 × 15 cm, and orthopyroxene (with abundant plagioclase lamellae) ranges up to 10 cm across. Such OPM clearly crystallized *in situ*, as their crystal form is largely defined by the geometry of surrounding grains of plagioclase (Fig. 6C). Plagioclase laths also occur as inclusions in OPM (Fig. 6B).

The relationship between these two "end-member" textural types on the outcrop scale is variable. Fairly sharp boundaries separate them in some places, whereas in others a gradation from coarse to fine (Fig. 6C) or schlieren of coarser material within finer types (Fig. 6A) are observed. Elsewhere, domains of texturally variable lithologies are juxtaposed in a confused way, with hints of layering present locally (Fig. 6D).

Petrography and mineral chemistry

Most of the orthopyroxene in the *coarse-grained leuconorite* comprises OPM, which occur as anhedral single crystals or crystal aggregates up to 10 cm across. The boundary between adjacent OPM in an

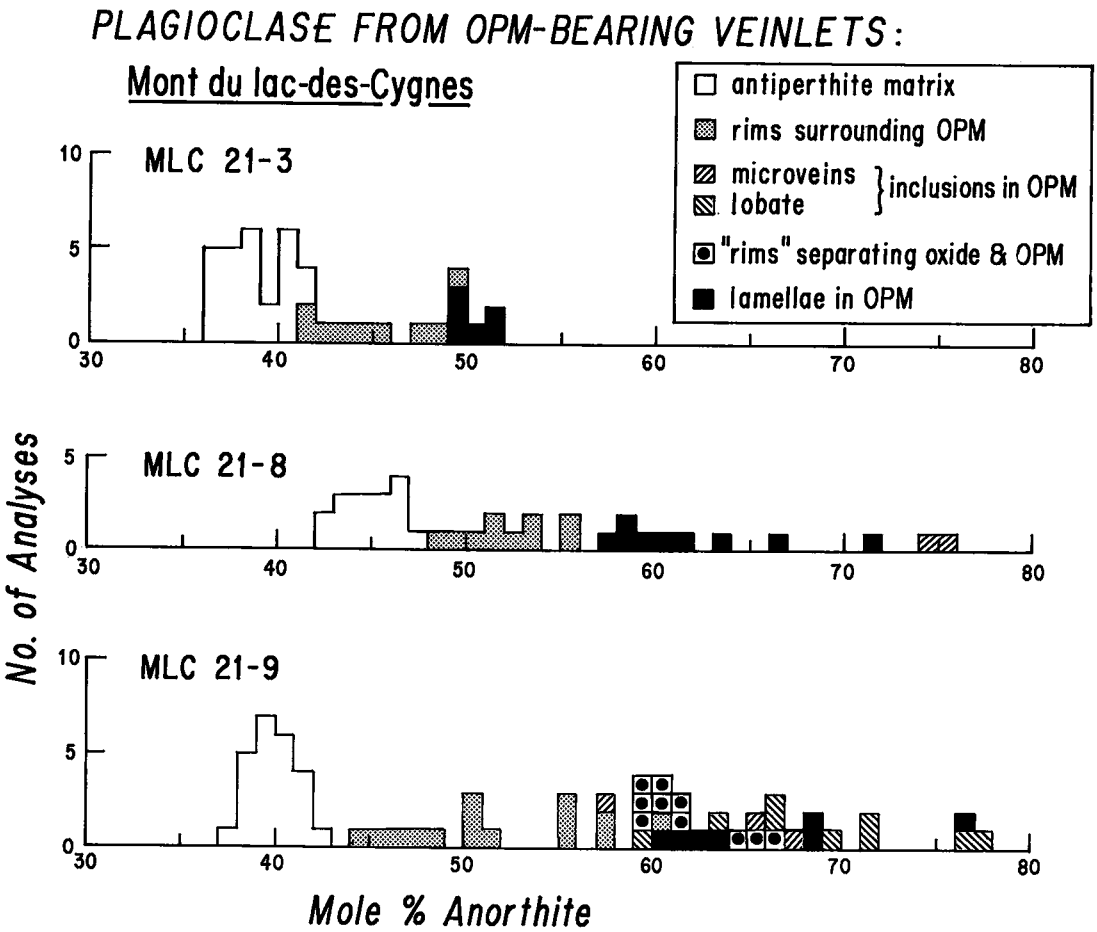

FIG. 5. Compositions of plagioclase from OPM-bearing veins; see text for description of types of plagioclase textures.

aggregate is not a sharp interface, but rather an irregular zone characterized by subequant, finer-grained (~0.5–1.0 mm) orthopyroxene, plagioclase, oxide and biotite. Some of this finer-grained orthopyroxene is kinked, and may have recrystallized from an OPM precursor.

The OPM contain abundant lamellae and inclusions of plagioclase and oxide, rare lamellae and "patches" of exsolved clinopyroxene and, in a very few cases, acicular biotite oriented parallel to the direction of elongation of the various types of lamellae (Fig. 7A).

OPM rims range from smooth to irregular and embayed, commonly by plagioclase and rarely by biotite. The plagioclase embayments are transitional to veinlike masses containing minor oxide and biotite. Where biotite occurs at the border of an OPM, it may contain tiny lenticular grains of orthopyroxene that are in optical continuity with each other and the OPM, suggesting magmatic replacement (Fig. 7B). Elsewhere, thin amoeboid protrusions extend from the OPM into the surrounding matrix; these are transitional to elongate grains of orthopyroxene (up to 1 mm long) occurring at boundaries of plagioclase grains in the matrix. Orthopyroxene also forms inclusions (< 100 μm wide) in matrix plagioclase, where they typically occur in clusters (Fig. 7C).

Despite their large size, the OPM are remarkably homogeneous (En_{70-72}, Fig. 8), but they do have a range of Al contents (~2.6–4.6 wt. % Al_2O_3). The rim is generally less aluminous than the core, and Al_2O_3 also is lower near plagioclase lamellae and inclusions. Orthopyroxene that occurs in the matrix and as inclusions in plagioclase is slightly more Fe-rich (En_{67-69}, Fig. 8) and less aluminous (~1.9–3.0 wt. %) than OPM.

Matrix plagioclase consists typically of 5–15 mm

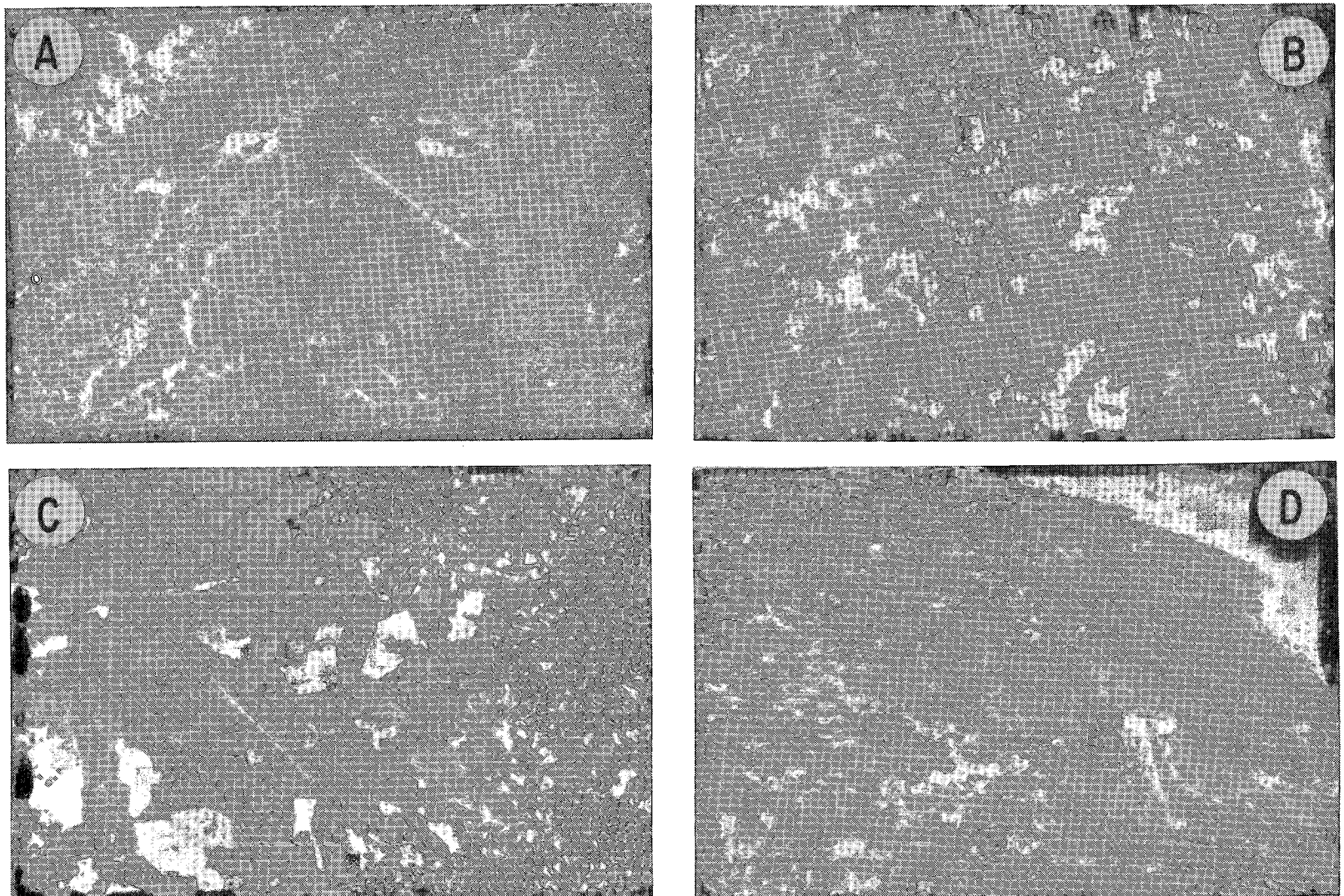

FIG. 6. Outcrop characteristics of leuconorites (locality B in Fig. 1). (A) Relatively homogeneous medium-grained leuconorite interspersed with patches of coarse-grained leuconorite. (B) Homogeneous coarse-grained leuconorite displaying well-developed subophitic texture. (C) Irregular "contact" between domains of leuconorites with contrasting grain-size; note angular form of OPM. (D) Irregular layering (?) in coarse- and medium-grained leuconorite.

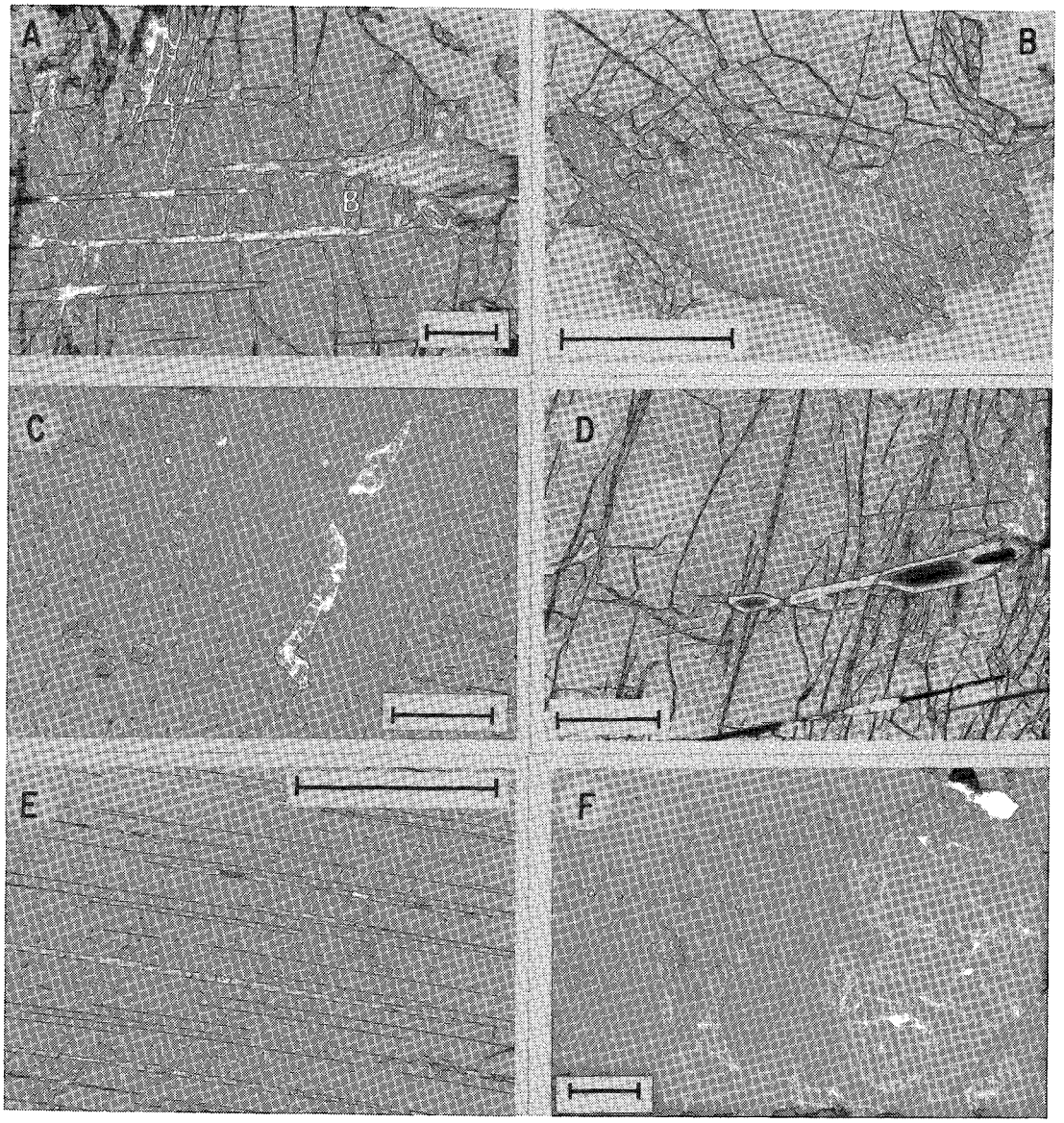

FIG. 7. Textural characteristics of various leuconorites. All bar scales represent 500 μm; D, E in cross-polarized light; others in plane-polarized light; sample numbers indicated. (A) Acicular inclusions of biotite (*B*) elongate parallel to lamellae orientation near OPM margin (CHV 80–99, 1). (B) OPM "replaced' by biotite; note tiny relics of pyroxene within biotite (CHV 80–97, 1). (C) Interstitial orthopyroxene, and orthopyroxene inclusions in plagioclase (CHV 80–99, 1). (D) Irregularly shaped lamellae segments of plagioclase displaying reversely zoned rims (CHV 80–99, 1). (E) Lamellae in OPM: plagioclase (broad, white), clinopyroxene (thin, white), oxide (dark); note that plagioclase lamellae are discontinuous and contain blocky segments of oxide (oxide is hemoilmenite; see text for discussion, CHV 80–99, 1). (F) Orthopyroxene in fine-grained leuconorite (CHV 80–97, 2).

polygonal grains with measured compositions in the range An_{37-43} (Fig. 9). Plagioclase adjacent to OPM is somewhat finer-grained (~1–3 mm), with compositions as calcic as An_{55} occurring in reversely zoned rims up to ~200 μm wide. Plagioclase with compositions An_{43-54} occurs in reversely zoned rims of similar width surrounding interstitial orthopyroxene, and around orthopyroxene inclusions in plagioclase.

Plagioclase lamellae (~5–50 μm wide) comprise

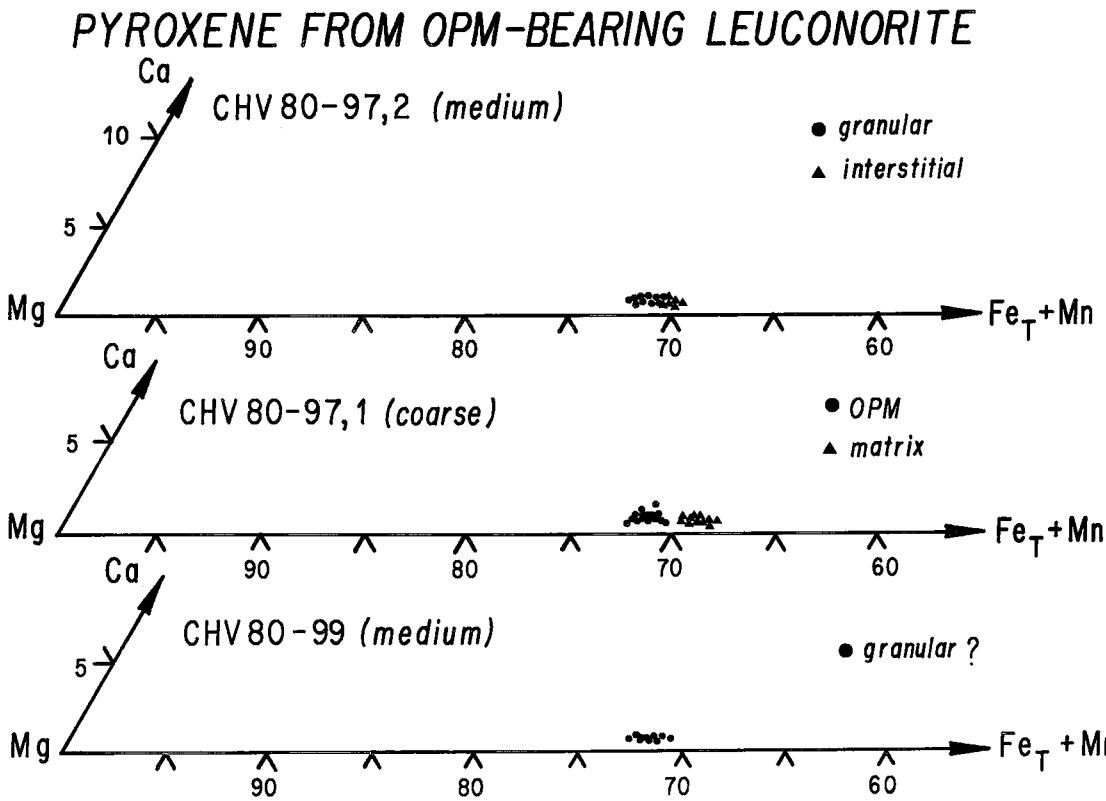

FIG. 8. Compositions of pyroxene in leuconorite; the data shown for CHV 80–99 (medium) pertain to a grain mount of the mineral separate used in the trace-element studies.

<5 % of the OPM. In the two samples studied in detail, these have measured compositional ranges of An_{54-59} and An_{71-89}, and are reversely zoned. The lamellae are all oriented parallel to (100) of the host, and are commonly twinned; the angle between the plagioclase (010) twin plane and the elongation of the lamellae ranges from ~30 to 90°. In most cases, segments of lamellae are occupied by blocky to elongate granules of oxide of the same width as the lamellae (Fig. 7E).

Some systematics in the distribution of lamellae are evident in that they are not observed to extend to the edge of any OPM, and are absent from the immediate vicinity of plagioclase inclusions. In some areas of OPM, lamellae are regularly spaced (~1 mm apart), elsewhere they are not.

The shapes of lamellae are highly variable (Fig. 7D, E): some are continuous for more than a centimetre and maintain a nearly constant width over this distance; some are discontinuous and blebby, having the appearance of "necked down" fluid inclusions; others are short and stubby with tapered ends. In a few cases, the oxide segments of lamellae have this tapered form as well. Some lamellae are distinctly curved; in one case, the OPM (210) cleavage trace and the (100) plagioclase – oxide – clinopyroxene orientation subtend a 75° arc, indicating extensive bending and warping after crystallization and exsolution; this is a relatively rare feature, however.

Plagioclase also occurs as subequant 100–200 μm inclusions in OPM. In a few cases, these form globular clusters up to 500 μm across that have a slight tendency to be elongate parallel to the orientation of the plagioclase lamellae. Oxide, and rarely apatite, occur in some of these clusters. Plagioclase inclusions have measured compositions of $\sim An_{50-58}$ and are reversely zoned.

OPM are not present in the *medium-grained leuconorite;* the orthopyroxene occurs mostly as subrounded, anhedral grains (~2–5 mm) with irregular scalloped borders (Fig. 7F). The measured compositional range is small (En_{70-72}, Fig. 8; ~2.8-3.8 wt. % Al_2O_3, Table 2), with cores and rims showing no consistent differences, although the most Al-rich types are found in cores. Orthopyroxene

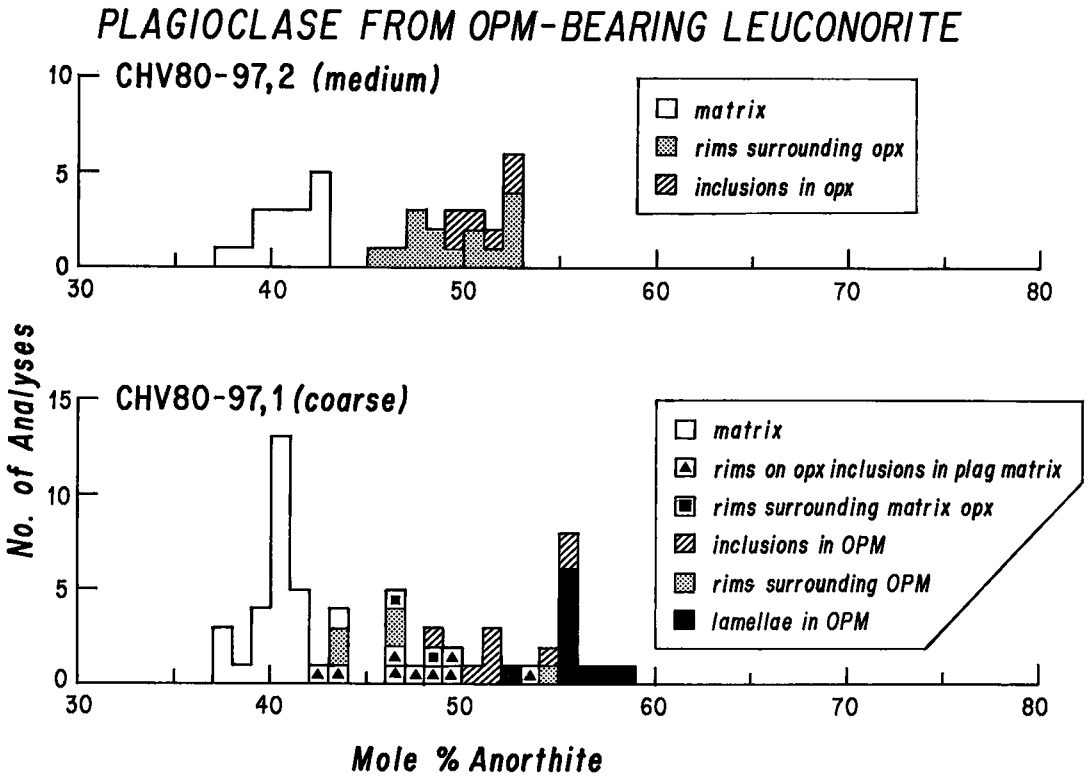

FIG. 9. Compositions of plagioclase in leuconorite; see text for description of texture types.

also forms smaller (~100–500 μm) angular grains interstitial to plagioclase (Fig. 7A), which are slightly less aluminous and more Fe-rich (~En_{69}, 1.8–2.9 wt. % Al_2O_3) than the larger grains.

Blocky inclusions of plagioclase (<200 μm) occur in some orthopyroxene grains, but no plagioclase lamellae were observed. Scattered inclusions (10–20 μm) and exsolved plates of hemoilmenite are also present. Clinopyroxene exsolution lamellae are very rare, and no discrete grains of clinopyroxene are present. Small flakes of biotite (~25 μm) occur at the margins of some orthopyroxene grains.

Plagioclase in the matrix comprises polygonal to irregularly shaped grains up to 5 mm across containing scattered needles of oxide and minor exsolved K-feldspar. Individual grains are homogeneous, but measured compositions are in the range An_{37-43} (Fig. 9). Rims adjacent to orthopyroxene (including the smaller interstitial matrix grains) are more calcic (An_{47-53}) and reversely zoned, in which the compositional change occurs gradually over a distance of ~400–500 μm. Inclusions in orthopyroxene (An_{49-53}) are also more calcic than matrix plagioclase, with slight reverse zoning.

OPM IN ANORTHOSITE

Field relations

At locality C (Fig. 1), anorthositic rocks have been identified as those that contain 5–10% scattered OPM ranging up to ~30 cm in maximum dimension (Fig. 10). These vary from blocky to elongated (‖*c*), with length/width ratios up to 5:1.

The plagioclase host ranges from dark grey, subequant megacrysts (up to 40 cm across) down to millimetre-sized pinkish brown aggregates. Most plagioclase megacrysts and some OPM are broken and crushed; rare OPM with prominent kink-bands have also been noted. Locally, plagioclase forms tabular megacrysts with interstitial, anhedral OPM. This subophitic texture indicates that at least some OPM from this association crystallized *in situ*. In general, however, these OPM-bearing anorthositic rocks appear massive.

Petrography and mineral chemistry

The petrographic characteristics of OPM from this lithology are largely similar to those in the coarse

TABLE 2. COMPOSITION OF PYROXENE FROM LEUCONORITE*

	1.	2.	3.	4.	5.	6.	7.	8.	9.	10.	11.	12.
Na_2O	0.02	0.03	0.01	0.00	0.00	0.00	0.06	0.68	0.00	0.00	0.01	0.00
MgO	24.72	25.93	24.45	24.50	24.10	25.18	25.81	12.91	25.14	25.54	25.71	25.67
Al_2O_3	3.92	2.86	2.21	2.62	2.55	4.58	4.11	6.86	3.44	2.63	1.84	3.28
SiO_2	52.15	53.33	52.80	52.44	52.39	51.62	52.13	47.48	52.12	52.83	53.26	52.14
CaO	0.39	0.23	0.25	0.33	0.36	0.27	0.34	23.08	0.31	0.30	0.24	0.35
TiO_2	0.16	0.09	0.10	0.07	0.16	0.09	0.10	1.10	0.09	0.11	0.07	0.07
Cr_2O_3	0.07	0.06	0.05	0.00	0.02	0.00	0.04	0.12	0.10	0.07	0.04	0.09
MnO	0.22	0.22	0.26	0.28	0.27	0.18	0.22	0.08	0.22	0.22	0.23	0.25
FeO_T	17.69	17.38	19.46	19.36	19.94	17.56	16.99	6.94	18.34	17.75	17.73	18.07
Total	99.34	100.13	99.59	99.60	99.79	99.48	99.80	99.25	99.77	99.45	99.13	99.92
FORMULA PROPORTIONS BASED ON 4 CATIONS AND 6 OXYGEN ATOMS												
Si	1.910	1.931	1.942	1.927	1.927	1.881	1.888	1.764	1.901	1.930	1.952	1.894
Al	0.090	0.069	0.058	0.073	0.073	0.119	0.112	0.236	0.089	0.070	0.048	0.106
Al	0.079	0.053	0.038	0.040	0.038	0.078	0.063	0.065	0.048	0.043	0.032	0.035
Cr	0.002	0.002	0.001	0.000	0.001	0.000	0.001	0.004	0.003	0.002	0.001	0.003
Fe 3+	0.002	0.012	0.014	0.030	0.026	0.037	0.042	0.155	0.043	0.019	0.012	0.064
Ti	0.004	0.002	0.003	0.002	0.004	0.002	0.003	0.031	0.002	0.003	0.002	0.002
Mg	1.349	1.399	1.341	1.342	1.321	1.368	1.394	0.715	1.367	1.391	1.405	1.390
Mn	0.007	0.007	0.008	0.009	0.009	0.005	0.007	0.003	0.007	0.007	0.007	0.008
Fe 2+	0.540	0.514	0.585	0.565	0.588	0.498	0.521	0.061	0.516	0.524	0.531	0.485
Ca	0.015	0.009	0.010	0.013	0.014	0.010	0.013	0.919	0.012	0.012	0.009	0.014
Na	0.001	0.002	0.001	0.000	0.000	0.000	0.004	0.049	0.000	0.000	0.001	0.000

COARSE-GRAINED LEUCONORITE

CHV80-97,1
1. *OPM core*
2. *OPM rim*
3. *Inclusion in biotite*
4. *Inclusion in plag*
5. *Interstitial*

CHV80-99,1
6. *OPM core*
7. *OPM core (near plag lamella)*
8. *Exsolved cpx bleb*

MEDIUM-GRAINED LEUCONORITE

CHV80-97,2
9. *Core*
10. *Rim*

CHV80-99,2
11. *Interstitial*
12. *Core*

**Based on microprobe analysis.*

leuconorite described above. Additional noteworthy features include the presence of 1–3 mm inclusions of oxide and plagioclase-rich veinlets near OPM margins (Fig. 11A). The oxide inclusions are typically separated from the enclosing OPM by a narrow layer of plagioclase (*cf.* Fig. 4C), whereas the OPM along the microveins appear to have recrystallized into granular aggregates (Fig. 11B). Plagioclase lamellae are virtually identical with those in the coarse leuconorite. Where kink bands occur in OPM, they are decorated by plagioclase blebs that appear to be recrystallized lamellae (Fig. 11C).

OPM are relatively homogeneous (En_{68-72}, Fig. 12), but have a range of Al contents (~2.0–4.7 wt. % Al_2O_3), with the lowest values near plagioclase lamellae and inclusions. In general, OPM rims and regions near veins are slightly more Fe-rich and less aluminous (En_{66-67}, 1.4–2.7 wt. % Al_2O_3), but compositional ranges overlap. Rare inclusions of orthopyroxene in matrix plagioclase are the most Fe-rich present (~En_{65}) and have the lowest Al contents (1.3–1.9 wt. % Al_2O_3).

Clinopyroxene of indeterminate composition comprises very thin exsolution lamellae in OPM. It also forms inclusions (50–100 mm) in matrix plagioclase (~$Ca_{48}Mg_{42}Fe_{10}$) and occurs as granules (<50 μm across) along plagioclase grain-boundaries (~$Ca_{48}Mg_{38}Fe_{14}$, Fig. 12); these types share a range of Al contents (1.5–3.9 wt. % Al_2O_3, Table 3), and have textures similar to clinopyroxene in the anorthositic veins.

Plagioclase compositions and textures are also similar to those in the coarse leuconorite. Matrix grains are in the range An_{38-42} (Fig. 13), whereas plagioclase lamellae and inclusions in OPM, rims on oxide inclusions in OPM, and rims around matrix orthopyroxene and OPM are more calcic (An_{42-78}) and reversely zoned. Plagioclase in the veinlets (An_{39-66}) has a core composition similar to that in the matrix, but is reversely zoned toward the enclosing OPM.

Rare-Earth-Element Characteristics

Sampling

Rare-earth element (*REE*) abundances were determined for OPM in samples of anorthosite and coarse-grained leuconorite. In each case, a single fragment (~10 g) was separated from a large (5–10 cm) OPM and powdered, with particular care taken to avoid or eliminate all surrounding material. These OPM fragments consist of orthopyroxene together with lamellae of clinopyroxene, plagioclase and oxide; separation of these phases was not possible. To the extent that such lamellae are exsolution products (see discussion below), the chemical characteristics of bulk OPM correspond to that of orthopyroxene at the time of its original crystallization from melt. Consequently, the *REE* concentrations in the OPM are considered most usefully along with their bulk chemical compositions (described below), rather than with the results of microprobe spot-analyses presented previously.

An orthopyroxene mineral separate was prepared from the medium-grained leuconorite to allow comparison of its *REE* abundances to those of the OPM in adjacent coarse-grained leuconorite. *REE* abundances were also determined for plagioclase from the OPM-bearing anorthosite, a plagioclase megacryst from the coarse-grained leuconorite, and a plagioclase separate from the medium-grained leuconorite. All of the *REE* data are presented in Table 4, and chondrite-normalized patterns are illustrated in Figures 14 to 16. Analytical techniques are described in the Appendix.

Results

Three OPM were analyzed from a single large (~0.5 m) sample of anorthosite (CHV 80–33; locality C in Fig. 1) to permit some assessment of their variability. As shown in Figure 14, these OPM possess similar and fairly low *REE* concentrations (<10 × chondrite). The pattern shapes are essentially parallel, with relatively flat heavy *REE* ($Gd_N \approx Yb_N$), and a pronounced fractionation in the light *REE* ($Ce_N < Sm_N$). In addition, the OPM all have a prominent negative Eu anomaly, with Eu/Eu* in the range 0.51–0.64 (where Eu* is the value interpolated from Sm and Gd).

An OPM from coarse-grained leuconorite and an orthopyroxene separate from medium-grained leuconorite were obtained from a single sample containing the contact between these two textural types (CHV 80–99; locality B in Fig. 1). The *REE* patterns of these two samples of orthopyroxene (Fig. 15) closely parallel each other, but their *REE* abundances differ by an order of magnitude. Each is characterized by relatively flat heavy *REE*, modest decreases in the light *REE*, and a large negative Eu anomaly (Eu/Eu* 0.38, 0.48). Compared to the OPM from the anorthosite, the orthopyroxene in leuconorite is less steeply sloped in the light *REE* and has a larger Eu anomaly. Nevertheless, a strong family resemblance among the shapes of the *REE* patterns is evident, and suggests that these orthopyroxene crystals shared many aspects of their origin.

The plagioclase and plagioclase-rich materials associated with the orthopyroxene have low *REE* abundances (<10 × chondrite) and strongly fractionated patterns (Ce_N/Yb_N in the range 25–150; Fig. 16). In the three samples analyzed, the abundances of the light *REE* and Eu are similar, but the patterns diverge considerably in the heavy *REE*. These differences appear to be related to the mineralogical purity of the different samples. The plagioclase separate from the medium-grained leuconorite, which has the lowest concentrations of the heavy *REE*, was highly purified and acid-washed. In contrast, the plagioclase megacryst from the coarse-grained leuconorite and the plagioclase-rich matrix from the anorthosite were analyzed in bulk and were not purified of the small quantities of other minerals found with them (excepting OPM). Petrographic observations indicate that no more than a few percent of other minerals are present, but the concentrations of the heavy *REE* in plagioclase are so low that even this amount of foreign material (with higher abundances of *REE*) could augment substantially the heavy-*REE* concentrations in the analyzed plagioclase. This appears to be confirmed

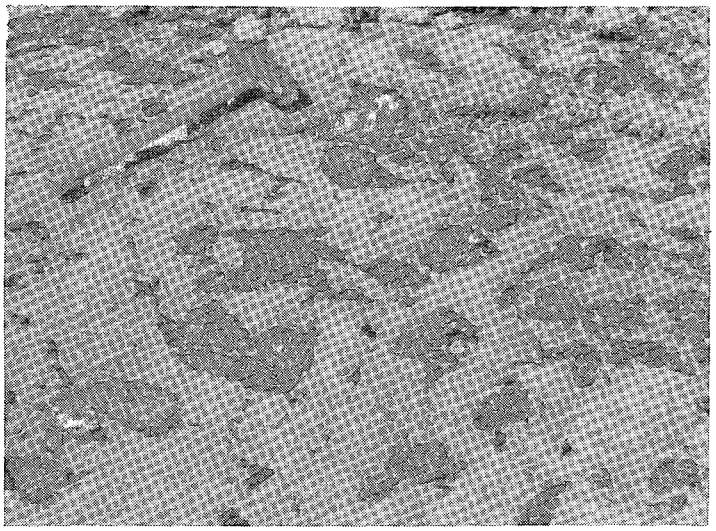

FIG. 10. Typical appearance of OPM-bearing anorthosite.

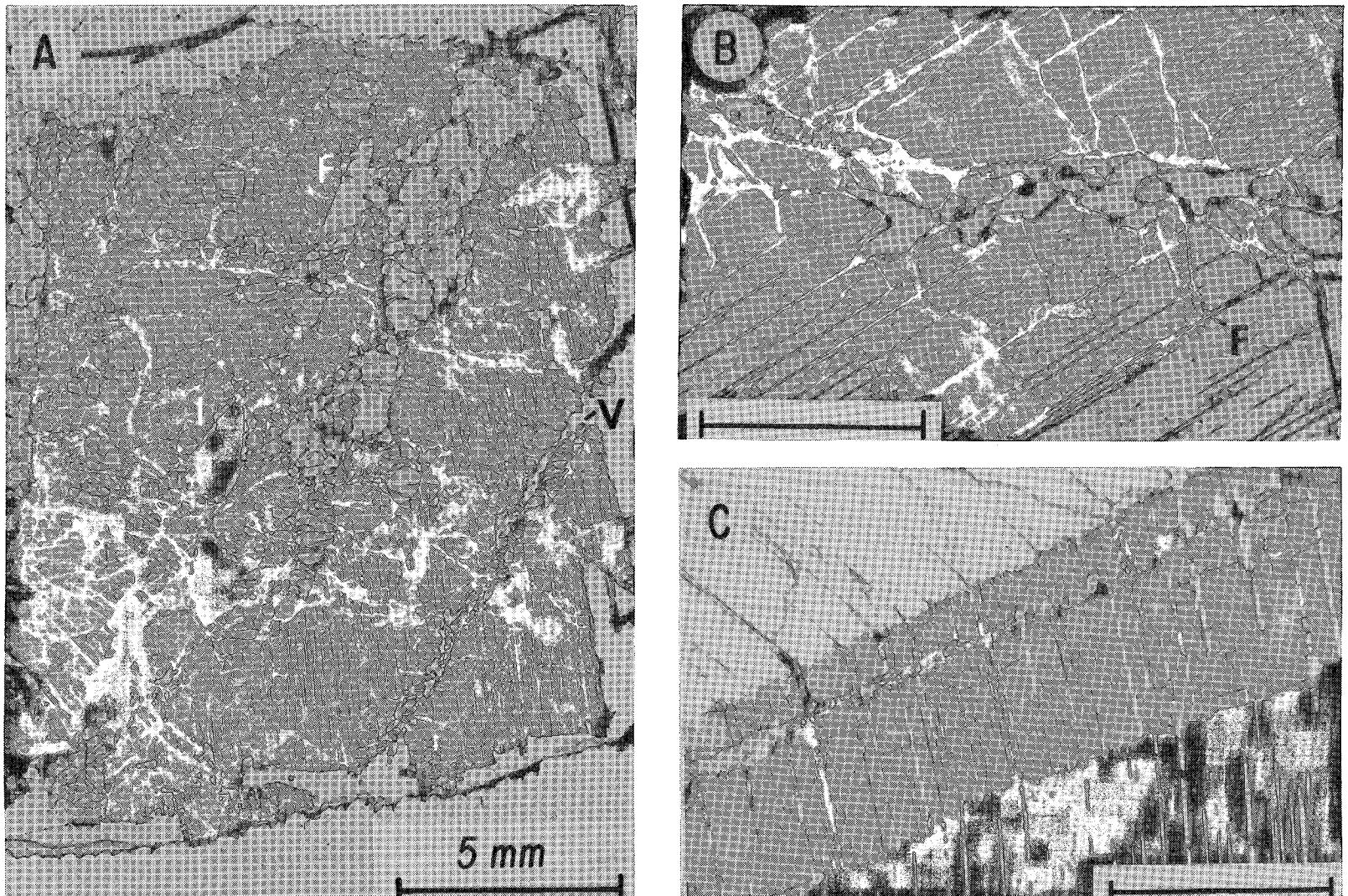

FIG. 11. Textural features of OPM in anorthosite (A, B in plane-polarized light, C in cross-polarized light; bar scales in B, C = 500 μm). (A) Enlarged view of a portion of an OPM; note cross-cutting plagioclase-rich veinlet (*V*), oxide inclusion (*I*) surrounded by plagioclase rim, and tabular inclusion of plagioclase(*F*) (STU 24–7). (B) Close-up view of plagioclase-rich veinlet illustrated in (A); note granular form of orthopyroxene in veinlet. Plagioclase lamellae (*F*) are also present here (STU 24–7). (C) Kink bands in OPM; note granular plagioclase decorating the kink bands and abundant plagioclase lamellae (CHV 80–33).

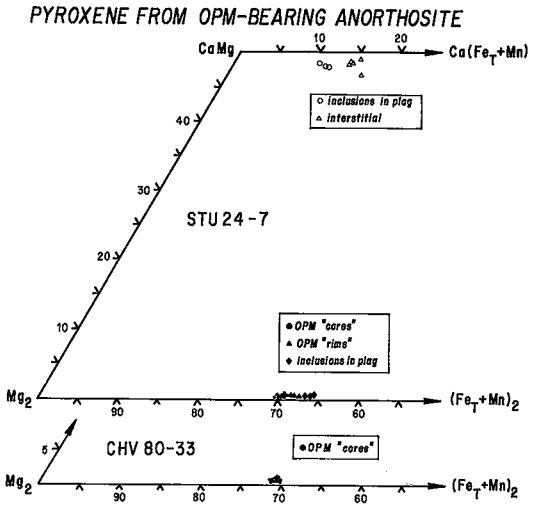

FIG. 12. Compositions of pyroxene in OPM-bearing anorthosites.

TABLE 3. COMPOSITION OF PYROXENE FROM ANORTHOSITE*

	1.	2.	3.	4.	5.	6.	7.	8.	9.
Na_2O	0.00	0.00	0.02	0.00	0.00	0.00	0.00	0.41	0.39
MgO	24.94	25.01	24.33	24.56	24.68	23.38	23.88	14.23	13.14
Al_2O_3	4.69	3.81	3.21	2.59	1.85	1.45	1.44	1.86	1.52
SiO_2	51.30	51.78	52.48	53.04	53.17	53.16	53.47	53.29	52.60
CaO	0.36	0.34	0.30	0.27	0.30	0.37	0.28	23.51	23.79
TiO_2	0.11	0.08	0.09	0.11	0.07	0.09	0.08	0.21	0.17
Cr_2O_3	0.13	0.07	0.08	0.07	0.07	0.04	0.04	0.04	0.01
MnO	0.28	0.25	0.23	0.30	0.30	0.36	0.28	0.12	0.27
FeO_T	18.67	18.07	19.05	19.06	19.39	21.34	20.86	7.20	8.82
Total	100.48	99.41	99.79	100.00	99.83	100.19	100.33	100.87	100.71
FORMULA PROPORTIONS BASED ON 4 CATIONS AND 6 OXYGEN ATOMS									
Si	1.858	1.894	1.923	1.941	1.951	1.962	1.965	1.956	1.949
Al	0.142	0.106	0.077	0.059	0.049	0.038	0.035	0.044	0.051
Al	0.059	0.058	0.062	0.052	0.031	0.025	0.028	0.036	0.015
Cr	0.004	0.002	0.002	0.002	0.002	0.001	0.001	0.001	0.000
Fe^{3+}	0.073	0.041	0.009	0.000	0.013	0.006	0.002	0.024	0.054
Ti	0.003	0.002	0.002	0.003	0.002	0.002	0.002	0.006	0.005
Mg	1.347	1.364	1.329	1.339	1.350	1.286	1.308	0.778	0.726
Mn	0.009	0.008	0.007	0.009	0.009	0.011	0.009	0.004	0.008
Fe^{2+}	0.492	0.512	0.575	0.583	0.582	0.653	0.639	0.197	0.219
Ca	0.014	0.013	0.012	0.011	0.012	0.015	0.011	0.924	0.944
Na	0.000	0.000	0.001	0.000	0.000	0.000	0.000	0.029	0.028

1. OPM core, CHV80-33
2. OPM core, CHV80-33
3. OPM core, STU24-7
4. OPM core, STU24-7
5. OPM rim, STU24-7
6. Opx inclusion in plag, STU24-7
7. OPM rim near veinlet, STU24-7
8. Cpx inclusion in plag, STU24-7
9. Interstitial cpx, STU24-7

*Based on microprobe analyses

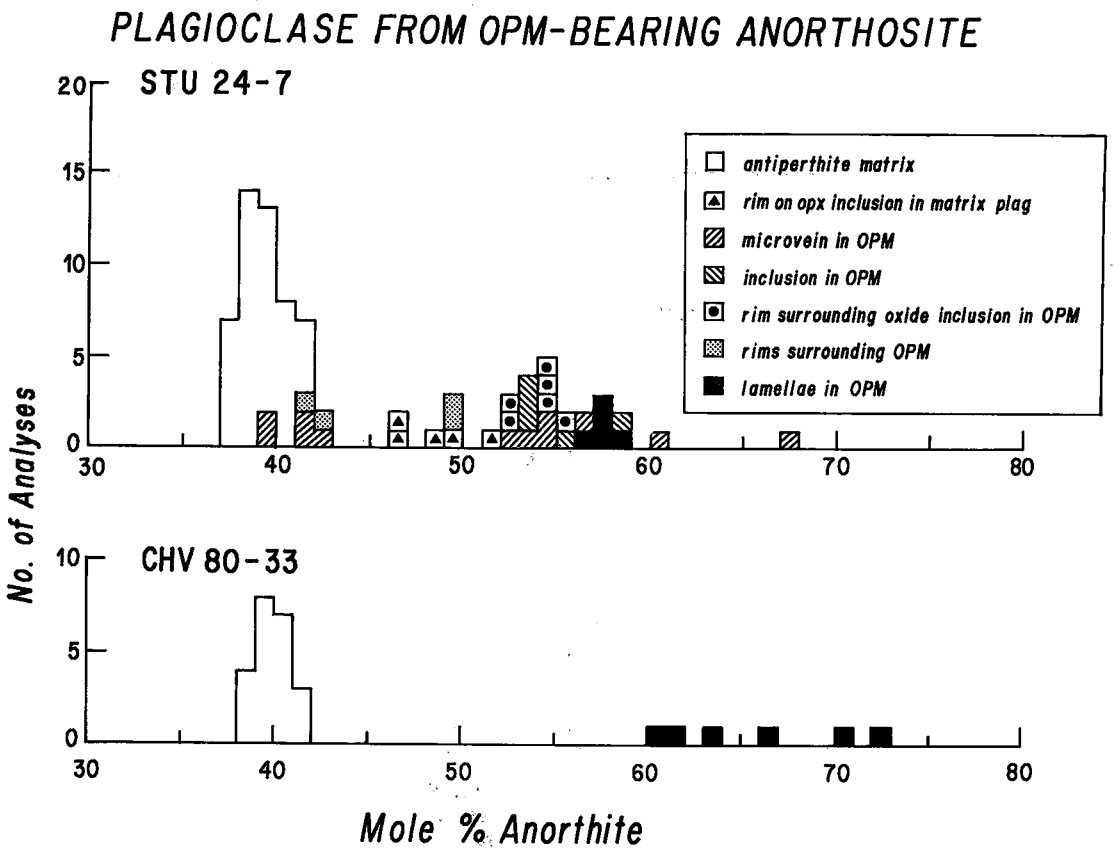

FIG. 13. Compositions of plagioclase in OPM-bearing anorthosites; see text for description of texture types.

TABLE 4. RARE-EARTH-ELEMENT ABUNDANCES (ppm)

	ORTHOPYROXENE					PLAGIOCLASE			
	1.	2.	3.	4.	5.	6.	7.	7a.	8.
Ce	0.899	0.585	1.15	3.47	0.369	4.39	4.26	3.58	3.62
Nd	1.60	1.21	1.46	3.85	0.378	2.13	2.30	1.65	1.93
Sm	0.920	0.694	0.820	1.57	0.149	0.323	0.407	0.229	0.309
Eu	0.216	0.192	0.188	0.301	0.0228	0.700	0.623	0.580	0.608
Gd	1.48	1.25	1.56	2.44	0.238	0.220	0.316	0.148	0.208
Dy	1.92	1.71	2.14	3.20	0.308	0.0941	0.179	0.0701	0.0696
Er	1.24	1.15	1.48	1.98	0.184	0.0301	0.0642	0.0234	0.0146
Yb	1.33	1.27	1.68	2.02	0.204	0.0175	0.0425	0.0198	0.00622

1. OPM A, 2. OPM B, 3. OPM C } *CHV80-33 Anorthosite*
4. OPM, CHV80-99,1 coarse leuconorite
5. Opx separate, CHV80-99,2 medium leuconorite
6. Plag matrix, anorthosite, CHV80-33
7. Plag megacryst, coarse leuconorite, CHV80-99,1
7a. Purified and acid washed powder from #7
8. Plag separate, medium leuconorite, CHV80-99,2

by the reduced heavy-*REE* concentrations in the plagioclase megacryst following purification and acid-washing (see Fig. 16). Overall, the principal characteristics of the *REE* data for plagioclase (low abundances, strong fractionation, large positive Eu anomalies with Eu/Eu* in the range 5.4–8.1) correspond closely to *REE* observed in andesine anorthosite throughout the St-Urbain massif (Gromet & Dymek 1980, 1981b).

Rb-Sr Relationships

Rb and Sr isotopic analyses were carried out on two of the OPM (1 each from anorthosite and coarse-grained leuconorite), the orthopyroxene separate from the medium-grained leuconorite, and plagioclase-rich materials associated with them. Elemental concentrations and isotopic ratios are listed in Table 5, and illustrated on a Rb-Sr evolu-

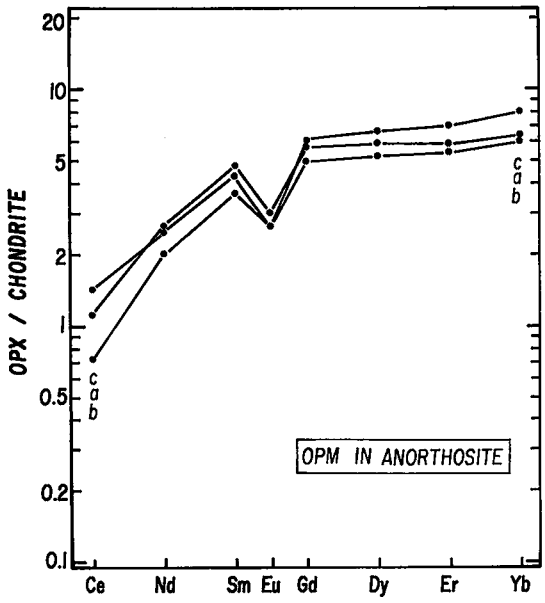

FIG. 14. *REE* patterns of three orthopyroxene megacrysts from anorthosite sample CHV 80-33. The letters a, b, c refer to those OPM for which bulk analyses are listed in Table 6 (#2–4); see text for additional discussion.

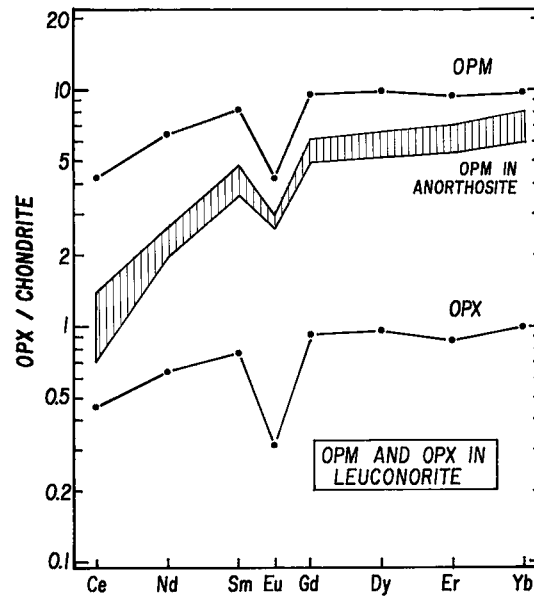

FIG. 15. *REE* patterns of an orthopyroxene megacryst from coarse-grained leuconorite (CHV 80-99, 1) and for an orthopyroxene separate from medium-grained leuconorite (CHV 80-99, 2); field of *REE* for the three OPM from anorthosite is shown for comparison.

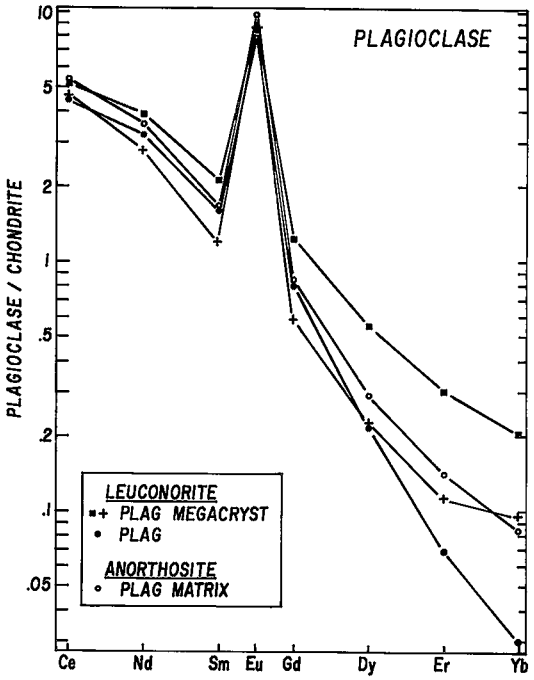

FIG. 16. *REE* patterns of a plagioclase megacryst from coarse-grained leuconorite CHV 80-99, 1 (■), the same megacryst following purification and acid washing (+), plagioclase from medium-grained leuconorite CHV 80-99, 2 (●), and plagioclase matrix from anorthosite CHV 80-33 (○).

tion diagram (Fig. 17).

The plagioclase-rich materials have nearly identical isotopic compositions ($^{87}Sr/^{86}Sr \simeq 0.7042$) and very high Sr concentrations (~1200 ppm). Rb/Sr ratios are very low, and indicate little radiogenic enrichment in $^{87}Sr/^{86}Sr$ over the probable age of the massif. The Sr isotopic ratios and Rb and Sr concentrations of these materials agree closely with those found in andesine anorthosites of the massif (Gromet & Dymek 1981b). The Sr isotope compositions of the various types of orthopyroxene show a range of values, however, and these do not correspond to variations in Rb/Sr ratios.

The slopes of lines connecting orthopyroxene and associated plagioclase correspond to "ages" of approximately 625, 1300 and 1700 Ma for the OPM in anorthosite (sample CHV 80-33), the OPM in coarse-grained leuconorite (CHV 80-99, 1), and orthopyroxene in medium-grained leuconorite (sample CHV 80-99, 2), respectively. The Rb-Sr "age" of the coarse-grained leuconorite (CHV 80-99, 1) does not differ greatly from the presumed age of the massif, but the calculated "ages" of the anorthosite (CHV 80-33) and the medium-grained leuconorite (CHV 80-99, 2) are significantly younger and older, respectively. The young age and the presence of some (minor) iron staining on the external and, to a lesser extent, internal cleavage-surfaces of the OPM in anorthosite suggest that it may have been a partially open system at some time relatively late in its history.

In summary, these results suggest that the Rb–Sr isotopic systems in orthopyroxene have been disturbed and are unreliable. The very low Rb and Sr concentrations in orthopyroxene (see Table 5) have undoubtedly contributed to this problem.

BULK COMPOSITIONS OF OPM

Bulk compositions of OPM were determined by microprobe analysis of fused glass prepared from aliquots of the same powders as used in the trace-element studies. Results are listed in Table 6, together with the average compositions from microprobe spot-analyses on grain mounts of the same orthopyroxene for comparative purposes.

The three OPM from sample CHV 80–33 have similar compositions, which are also similar to the OPM from sample CHV 80–99. As a group, bulk OPM are characterized by a relatively high content of Al (~ 5 wt. % Al_2O_3) and only a limited range in Mg/(Mg + Fe), from 0.69 to 0.72. Compared to spot analyses, bulk OPM have lower contents of Mg and Si but are enriched in Na, Al, Ca, Ti, and, to a lesser extent, Fe. These differences clearly reflect the contributions from plagioclase, oxide and clinopyroxene lamellae to the bulk composition of the orthopyroxene megacrysts. The values for Mn and Cr are too low to permit an unambiguous assessment of any changes in concentrations.

The reconstituted bulk-compositions of the OPM yield reasonably good pyroxene-type R_2O_3 stoichiometry. However, the abundance of various lamellae is sufficiently low that any departures from

TABLE 5. Rb-Sr ISOTOPIC DATA*

Sample	Rb (ppm)	Sr (ppm)	$^{87}Rb/^{86}Sr$	$^{87}Sr/^{86}Sr$
1. OPM A from anorthosite sample CHV80-33	0.423	12.0	0.102	0.70509±6
2. OPM from coarse-grained leuconorite CHV80-99,1	0.898	21.9	0.119	0.70624±4
3. Opx from medium-grained leuconorite CHV80-99,2	0.192	5.35	0.104	0.70661±3
4. Plagioclase from anorthosite CHV80-33	3.19	1214.	0.00759	0.70425±6
5. Plag megacryst from coarse-grained leuconorite CHV80-99,1	3.35	1178.	0.00822	0.70419±6
6. Plag concentrate from medium-grained leuconorite CHV80-99,2	1.97	1172.	0.00487	0.70419±4

*Eight analyses of the NBS 987 Sr isotopic standard over a ten-month period including the interval during which this study was performed varied from 0.71049±4 (2σm) to 0.71056±4, and averaged 0.71052. These values are approximately 0.0003 higher than those obtained by most other laboratories, which should be taken into consideration in comparing the data reported here to the work of others.

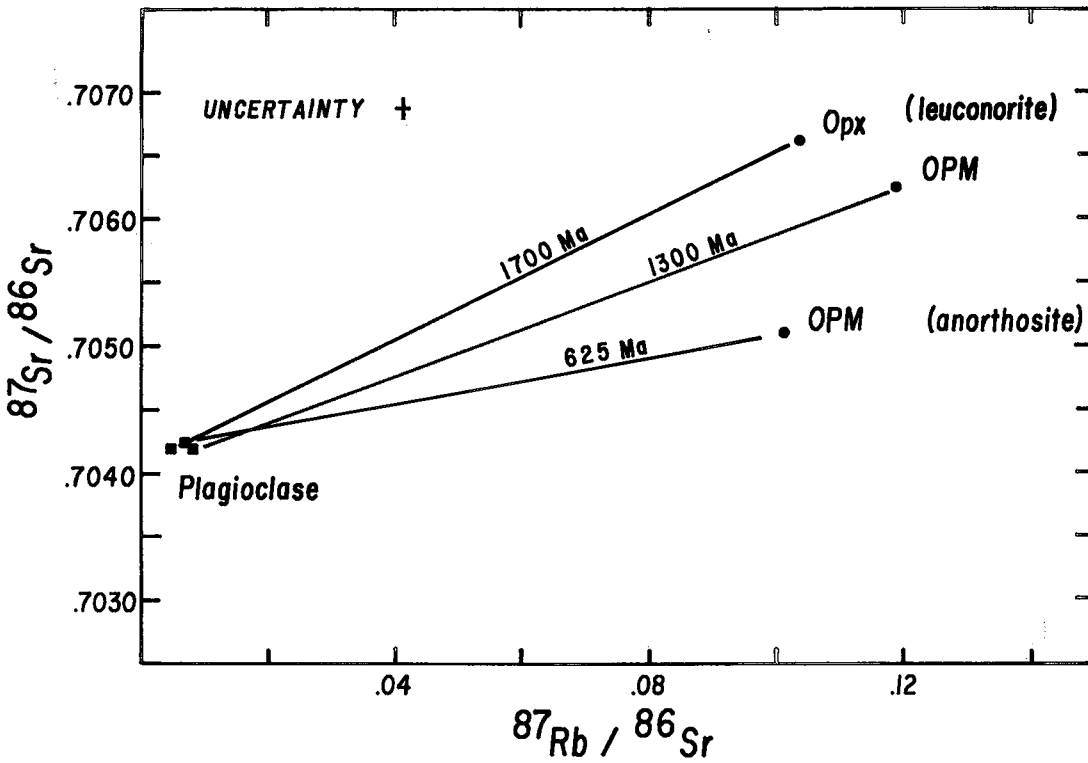

FIG. 17. Rb–Sr evolution diagram displaying plagioclase–orthopyroxene pairs from medium-grained leuconorite CHV 80–99, 1 (plag–opx), coarse-grained leuconorite CHV 80–99, 2 (plag–OPM) and anorthosite CHV 80–33 (plag–OPM). Ages calculated from the slopes of each pair are shown, but the temporal significance of these "dates" is uncertain (see text for discussion).

stoichiometry are probably not detectable by the method used for analysis. A comparison of cation abundances in bulk OPM and OPM spot-analyses reveals several interesting features. Figure 18 is a diagrammatic representation of charge-balance relationships for orthopyroxene in sample CHV 80–33. In bulk OPM, a large proportion of the Al occurs in tetrahedral co-ordination, where it compensates for R^{3+} and R^{4+} cations in octahedral co-ordination. The low content of Na limits the abundance of a possible jadeite component to a few percent at most. The amount of Fe^{3+} shown, which was arrived at by calculation and therefore subject to considerable uncertainty, corresponds to an Fe^{3+}/Fe_T ratio of ~0.15. However, the latter is in good agreement with a value of 0.18 determined by a potassium metavanadate titration. The OPM spot-analyses yield lower ^{iv}Al and Fe^{3+}, but ^{vi}Al is similar to bulk OPM. Important characteristics of the two data sets include the dominance of ^{iv}Al over ^{vi}Al and similar values of $Mg/(Mg + Fe_T)$ (*cf.* Table 6).

DISCUSSION

Overview

The characteristics of the OPM described in this report appear to reflect several different and generally complex processes. The conspicuous presence of plagioclase (+ oxide + clinopyroxene) lamellae within OPM suggests that exsolution has been important in modifying an originally aluminous orthopyroxene. In addition to the exsolution process, other intriguing questions concerning the OPM include the circumstances of their original crystallization and the way these influenced OPM compositions, the nature of the magmas from which the OPM formed, and their relationship to the anorthositic host-rocks. However, insight into the igneous petrogenesis of the OPM may be developed by first evaluating the causes and consequences of the exsolution process. In the following sections, we address each of these topics, but in order to facilitate discussion, we begin with a brief summary of chemical data on minerals.

TABLE 6. COMPOSITION OF ORTHOPYROXENE MEGACRYSTS*

	1.	2.	3.	4.	5.	6.
Na_2O	0.03 (.02)	0.13 (.02)	0.10 (.04)	0.19 (.03)	0.03 (.03)	0.18 (.02)
MgO	24.87 (.17)	23.90 (.21)	23.99 (.39)	22.90 (.13)	25.59 (.31)	23.71 (.24)
Al_2O_3	4.03 (.21)	4.99 (.04)	5.20 (.06)	5.12 (.07)	4.34 (.34)	5.42 (.06)
SiO_2	51.44 (.22)	50.08 (.24)	50.04 (.42)	50.68 (.27)	51.75 (.42)	50.24 (.32)
CaO	0.34 (.02)	1.31 (.02)	1.38 (.04)	1.49 (.04)	0.42 (.10)	1.29 (.02)
TiO_2	0.10 (.02)	0.69 (.02)	0.70 (.05)	0.76 (.04)	0.13 (.09)	0.80 (.03)
Cr_2O_3	0.08 (.02)	0.09 (.03)	0.09 (.04)	0.15 (.04)	0.05 (.02)	0.09 (.03)
MnO	0.24 (.01)	0.22 (.03)	0.24 (.04)	0.25 (.04)	0.20 (.04)	0.22 (.04)
FeO_T	18.10 (.13)	18.56 (.18)	18.20 (.29)	18.44 (.29)	17.07 (.37)	17.91 (.25)
FORMULA PROPORTIONS BASED ON 4 CATIONS AND 6 OXYGEN ATOMS						
Si	1.885	1.829	1.826	1.857	1.880	1.835
Al	0.115	0.171	0.174	0.143	0.120	0.165
Al	0.059	0.044	0.050	0.079	0.066	0.068
Cr	0.002	0.003	0.003	0.004	0.001	0.003
Fe^{3+}	0.050	0.096	0.091	0.031	0.047	0.064
Ti	0.003	0.019	0.019	0.021	0.004	0.022
Mg	1.358	1.301	1.305	1.251	1.386	1.291
Mn	0.007	0.007	0.007	0.008	0.006	0.007
Fe^{2+}	0.505	0.470	0.465	0.534	0.471	0.483
Ca	0.013	0.051	0.054	0.059	0.016	0.050
Na	0.002	0.009	0.007	0.014	0.002	0.013

1. Anorthosite CHV80-33, OPM A, spot average (Weighted average ± 1σ for 2 sets of 15 analyses on grain mount).

2. Anorthosite CHV80-33, OPM A, bulk composition (Weighted average ± 1σ for 2 sets of 15 analyses on glass).

3. Anorthosite CHV80-33, OPM B, bulk composition (Average ± 1σ for 15 analyses on glass).

4. Anorthosite CHV80-33, OPM C, bulk composition (Weighted average ± 1σ for 2 sets of 15 analyses on glass).

5. Leuconorite CHV80-99, OPM, spot average (Average ± 1σ for 15 analyses on grain mount).

6. Leuconorite CHV80-99, OPM, bulk composition (Weighted average ± 1σ for 2 sets of 15 analyses on glass).

** Based on microprobe analyses; see Appendix for methods of bulk analysis.*

Inferences from mineral chemistry

The compositions of *orthopyroxene* in all samples from the St-Urbain massif studied to date are summarized in Figures 19 and 20, which illustrate that only a limited range in $Mg/(Mg + Fe_T)$ is observed. In these diagrams, "matrix" refers to non-OPM compositions, whereas for OPM, "spot" and "bulk" refer to results of point and fused-glass analyses, respectively, obtained by microprobe.

On an outcrop scale, some OPM have compositions that extend to slightly higher values of $Mg/(Mg + Fe_T)$ than associated matrix orthopyroxene (Figs. 19A, C, E), whereas others have equivalent compositions (Figs. 19C, D). Despite these slight differences, one of the most important features of the chemistry of orthopyroxene is that OPM have values of $Mg/(Mg + Fe_T)$ within the range of other orthopyroxene types in the massif as a whole. This observation extends to the OPM bulk compositions as well. In contrast, the Ca and Al contents of bulk OPM are distinctly higher than other orthopyroxene. Al contents from spot analyses of OPM also range to higher values although, in general, a continuum of compositions occurs with Al content decreasing with $Mg/(Mg + Fe_T)$.

These observations emphasize that Ca and Al contents, not Mg/Fe ratio, distinguish bulk OPM from other types of orthopyroxene at St-Urbain. This is of considerable significance because if En content is regarded as an index of timing of crystallization for the OPM relative to other orthopyroxene, then the data contraindicate a separate, early formation for OPM. Moreover, the nearly identical contents of En in orthopyroxene from coarse- and medium-grained leuconorite, where field relationships suggest *in situ* crystallization (*cf.* Fig. 6), and their similarity to the En content of OPM from the anorthosite (compare Figs. 8, 12 and Figs. 19C, D, E), collectively indicate that OPM crystallized along with other grains of orthopyroxene in the outcrops where they presently reside. In our opinion, the "problem"

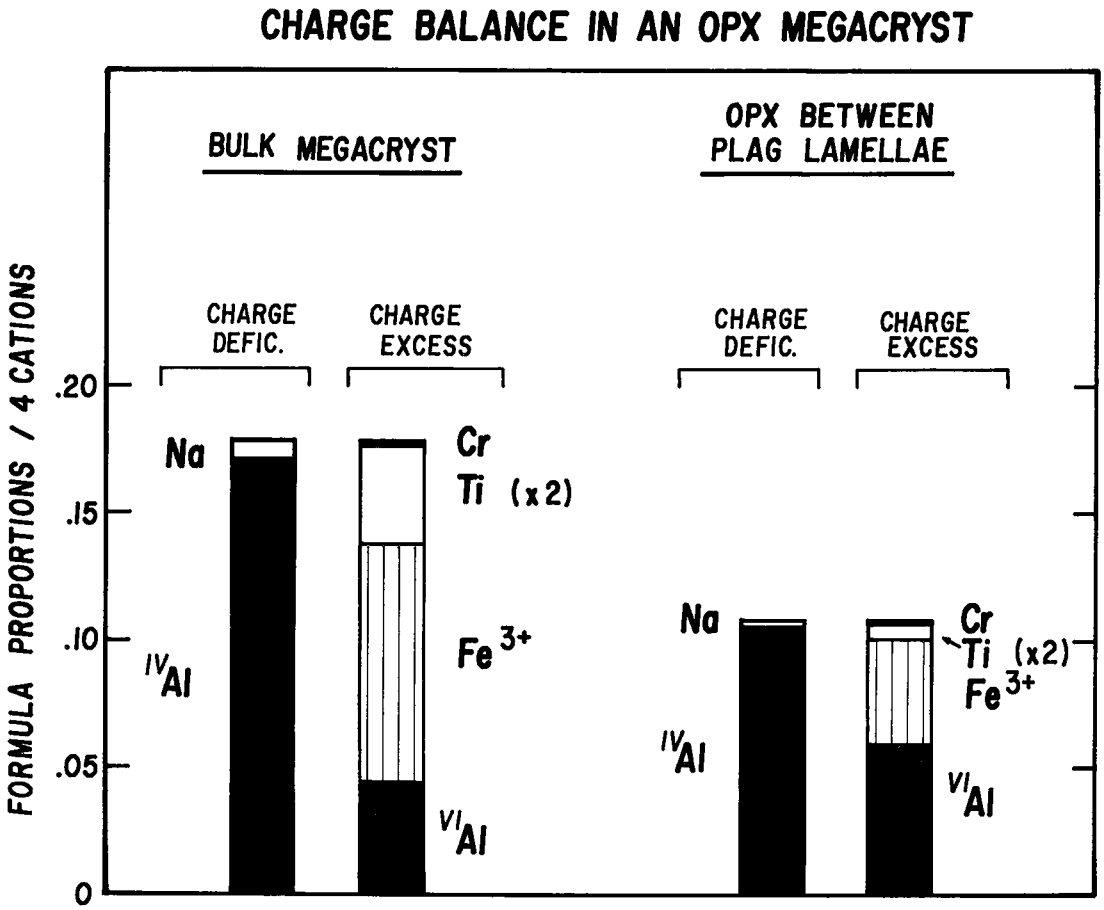

FIG. 18. Diagram illustrating cation abundances and corresponding charge-balance relationships for an orthopyroxene megacryst. Data are shown for OPM A in anorthosite sample CHV 80–33 (see text for discussion).

of OPM is not where they crystallized, but why they contain such "high" contents of Ca and Al.

In each of the three modes of occurrence of OPM, the *plagioclase* lamellae contained in OPM (An_{50-86}) are invariably more calcic than the matrix plagioclase (An_{37-45}). These relationships are summarized in Figure 21, where it can also be seen that there is an extensive overlap in the range of lamellae compositions from the different associations. Optical examinations indicate that the lamellae have in fact a somewhat wider compositional range than shown; additional analytical data could show complete overlap.

Although plagioclase lamellae tend to be the most calcic types in each sample studied, their An contents are approached (or even exceeded) by plagioclase inclusions in OPM, and by reversely zoned matrix plagioclase (*cf.* Figs. 5, 9, 13). It appears from textural considerations that the occurrence of reversely zoned plagioclase is related spatially to the presence of (largely interstitial) mafic minerals and other accessory phases, and not solely to the presence of OPM with plagioclase lamellae. For example, reverse zoning in plagioclase is found in the medium-grained leuconorite, which lacks OPM. It is also noteworthy that reverse zoning occurs against pyroxene inclusions in plagioclase. As discussed below, the development of reverse zoning in plagioclase may be linked to the same mechanism that produces lamellae in OPM.

Origin of plagioclase lamellae

Most, if not all, of the features that led Emslie (1975) and Morse (1975) to postulate an exsolution origin for the plagioclase lamellae are relevant to the St-Urbain OPM. These include: (1) approximate regularity of lamellae spacing, and regularity in their orientation, (2) variability of (010) twin-plane orientations of lamellae with respect to their boundaries, (3) lamellae compositions more calcic than the

matrix, (4) oxide segments in lamellae, (5) reverse zoning of lamellae, (6) slight Al depletion in OPM adjacent to lamellae.

We concur with Emslie and Morse that the plagioclase lamellae probably represent an exsolution phenomenon. However, the possibility that several of the above features owe their origin to some combination of igneous or subsolidus reactions other than to exsolution should not be dismissed without discussion. For example, the fact that reverse-zoning relationships are observed along plagioclase–pyroxene contacts at OPM margins and surround indisputable plagioclase inclusions in OPM, and that such plagioclase inclusions range to compositions as calcic as the lamellae, suggest that items 3, 5 and 6 are not unique to an origin by exsolution.

One alternative hypothesis is that reverse zoning in plagioclase lamellae and Al depletion in adjacent orthopyroxene result from subsolidus equilibration between orthopyroxene host and lamella-shaped inclusions of plagioclase that crystallized directly from a melt. In this case the regularity of lamella orientation [parallel to (100)] may merely reflect attachment of plagioclase crystals to an orthopyroxene surface advancing by step growth ⊥(100). One can envision the situation in which orthopyroxene crystallization results in the development of an Al-enriched boundary layer, thereby causing local supersaturation in plagioclase. Periodic nucleation and growth of plagioclase could be the cause of the approximately regular spacing of lamellae, in which diffusion rates of various melt-species played an important role. Such chemical boundary-layers have been produced experimentally adjacent to olivine (*e.g.*, Powell *et al.* 1980), and *qualitatively* similar effects could be expected adjacent to rapidly growing orthopyroxene.

The feature that is most damaging to the hypothesis that plagioclase lamellae are inclusions is also the one explained most elegantly by exsolution: the common occurrence of oxide grains as integral segments of the plagioclase lamellae. Although a rapidly advancing "front" of crystallization associated with growth of orthopyroxene locally could supersaturate the adjacent melt in oxide as well as plagioclase, this does not explain why these phases, which generally exhibit different habits, share the same contiguous lamellar form of constant width over distances of up to several millimetres. We consider this textural feature to be compelling evidence for a common origin by exsolution for both plagioclase and oxide in these lamellae, but the exact circumstances leading to the exsolution of these phases is problematical.

The principal difficulty is identifying how the plagioclase now represented by the lamellae was originally dissolved in the pyroxene. A high T–P pyroxene–plagioclase solid solution seems unlikely

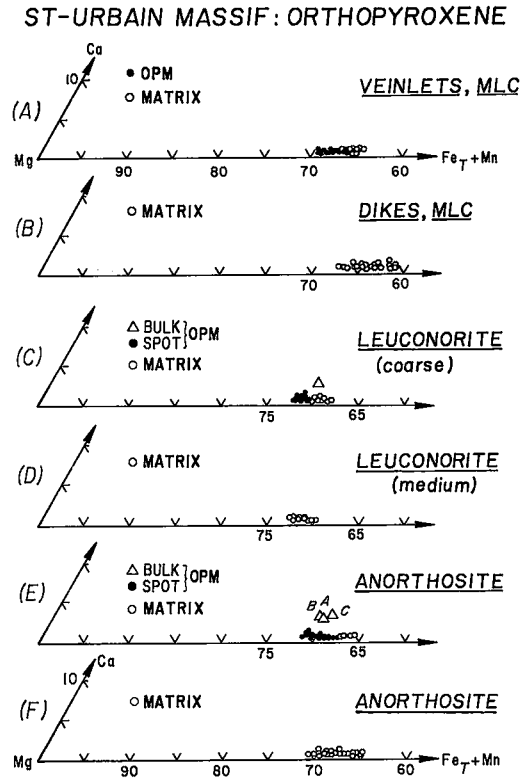

FIG. 19. Diagram summarizing available data on the compositions of orthopyroxene in various *andesine* anorthosites and leuconorites from the St-Urbain massif in terms of relative atomic percent Ca – Mg – (Fe_T + Mn); A, C, D, E refer to samples described in this report, whereas B and F represent unpublished data.

from the standpoint of mutually incompatible crystal-structures. An alternative is that minor-element ("nonquadrilateral") components originally present in the orthopyroxene decomposed to form plagioclase and other exsolution products upon cooling from magmatic conditions.

Emslie (1975) suggested that plagioclase lamellae result from unmixing of $CaAlSiAlO_6$ and $NaAlSi_2O_6$ components. This hypothesis could explain, in part, the calcic composition of lamellae since orthopyroxene would be expected to incorporate Ca components over Na components, but removal of these components in the form of plagioclase requires the addition of silica (*i.e.*, $CaAlSiAlO_6 + SiO_2 = CaAl_2Si_2O_8$ or Pyx + Silica = Plag). Morse (1975) addressed this dilemma by noting that exsolution of plagioclase from pyroxene could be viewed as the product of coupled reactions, and postulated that the requisite amount of silica could be produced by oxidation of ferrous pyroxene yielding magnetite in

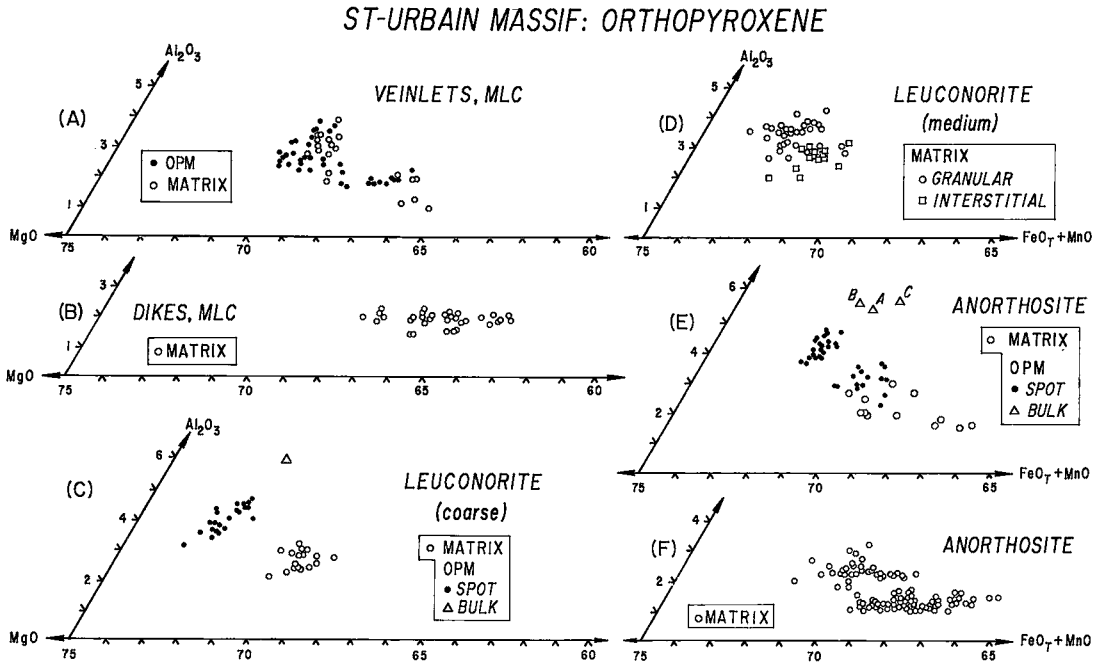

FIG. 20. Diagram summarizing composition of St-Urbain orthopyroxene in terms of relative mole percent MgO – Al_2O_3 – (FeO_T + MnO); divisions as in Figure 19.

addition (*e.g.*, $3FeSiO_3 + \frac{1}{2}O_2 = 3SiO_2 + Fe_3O_4$). This mechanism is rather attractive, as it also explains the magnetite associated with plagioclase lamellae in the Nain OPM. Bohlen & Essene (1978) also favored oxidation as a source of silica in the Adirondack OPM.

The occurrences of OPM at St-Urbain have an important difference in that the oxide associated with plagioclase lamellae (as well as that found as thin exsolved plates in OPM and as discrete grains throughout the samples) is hemoilmenite, not magnetite. (In only one sample, MLC 21-9, magnetite has been observed; it is intimately associated with pyrite, probably related to "alteration" of magmatic pyrrhotite at low temperatures.) The oxidation mechanism does not explain why a Ti-rich phase such as hemoilmenite is involved in the present case rather than a relatively pure hematite or magnetite; other mechanisms that do explain this feature should be considered.

The intimate association of hemoilmenite with plagioclase occupying alternate segments of the same lamellae is a compelling argument that oxide exsolution is a necessary and important part of the plagioclase lamella-forming process. A potentially important mechanism not involving oxidation is the decomposition of FeTi components in pyroxene, where:

$$R^{2+}_2\ Fe^{2+}Ti^{4+}Si_2Al_2O_{12} = FeTiO_3 + R^{2+}AlSiAlO_6 + R^{2+}SiO_3 \quad (1a)$$

$$R^{2+}_2\ Fe^{3+}_2Si_2Al_2O_{12} = Fe_2O_3 + R^{2+}AlSiAlO_6 + R^{2+}SiO_3 \quad (1b)$$

This mechanism is attractive in that Tschermak components are "liberated" by oxide exsolution, which may contribute to the formation of plagioclase lamellae; however, a source of silica is still needed.

Quartz occurs in minor myrmekitic intergrowths throughout the anorthositic matrix of most samples, but there is no compelling textural evidence for "migration" of silica from these regions into the megacrysts. An alternative source of silica may lie in certain vacancy-bearing or Eskola components (*cf.* Gasparik & Lindsley 1980b), as illustrated by the following reaction:

$$2[Ca_{0.5}\square_{0.5}AlSi_2O_6] = CaAl_2Si_2O_8 + 2SiO_2 \quad (2)$$

Decomposition of an Eskola component leads directly to plagioclase and produces silica, which can combine with Tschermak components (including those formed by oxide exsolution) to yield additional

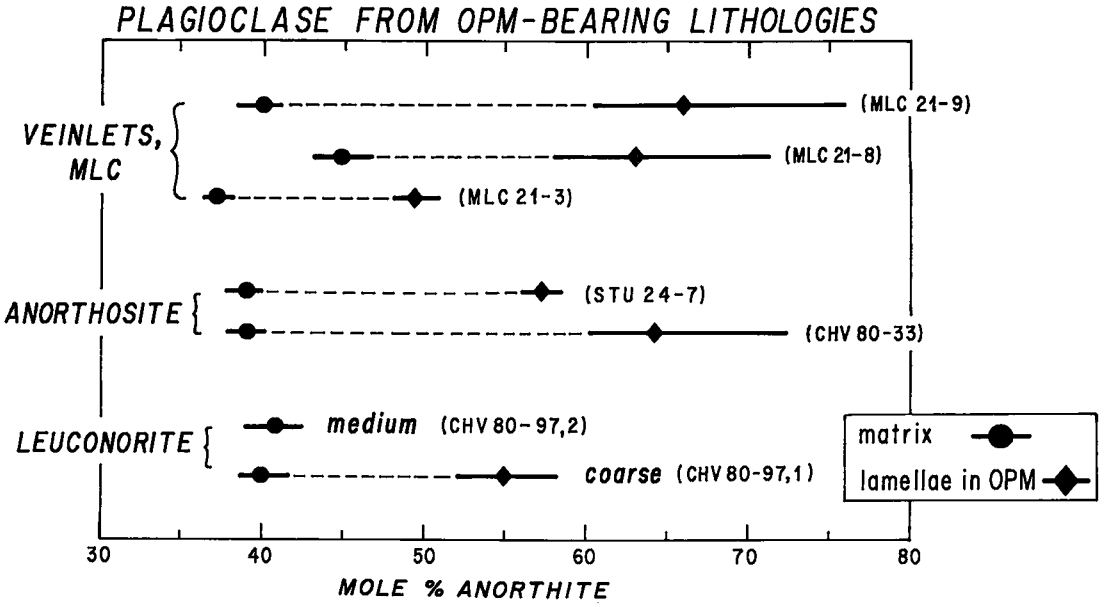

FIG. 21. Diagram comparing compositions of plagioclase lamellae and matrix plagioclase in OPM-bearing samples described in this paper.

plagioclase. A sodic analogue of the Eskola component is not known and seems unrealistic, as it would necessitate octahedral Si for charge balance. This by itself may explain the calcic nature of the lamellae, since 2 moles of Ca-Eskola component can yield 3 moles of plagioclase, one of which must be anorthite. This sets a "natural" lower compositional limit of An_{33} for the exsolved plagioclase.

The occurrence of a vacancy-type substitution requires that the original pyroxene be nonstoichiometric, a feature that we cannot verify. However, an approximate value of the abundance of vacancies that would be required can be estimated from the difference in Ca and Na between bulk OPM and spot compositions, which corresponds to ~0.045 cations/formula unit (*cf.* Table 6). If one third of these were involved in an Eskola component (see eqn. 2), then there would be ~0.015 vacancies/formula; this limited deviation from stoichiometry is not detectable by our analytical methods.

In summary, no mechanism for producing plagioclase from pyroxene is entirely satisfactory, but the simultaneous decomposition of vacancy- and Fe–Ti-bearing components appears capable of explaining many of the unusual chemical and textural features of the OPM, especially the association of oxide with plagioclase in individual lamellae. Thus, the abundance of plagioclase lamellae may not be controlled strictly by the abundance of original Tschermak and Jadeite components, but by metastable vacancy-bearing components. Oxidation does not seem to be required specifically in the exsolution process, as observed at St-Urbain, although it may have contributed to exsolution in other OPM occurrences.

The presence of reversely zoned plagioclase at all OPM borders, and the absence of plagioclase lamellae there and around plagioclase inclusions in OPM, are features that may be related to the same process that led to the formation of lamellae; on the one hand, plagioclase exsolved as lamellae throughout OPM, but at grain boundaries, this exsolving plagioclase "plated out" against inclusions or external contacts of the grains (*i.e.*, a limited type of granular exsolution). The occurrence of thin layers of calcic plagioclase along OPM–oxide boundaries and around inclusions of oxide in OPM (*i.e.*, locations where the exsolved plagioclase could not combine or mix with pre-existing plagioclase) provides rather convincing evidence that such a process occurred (*cf.* Figs. 3C, 11A).

Origin of the composition of OPM

If plagioclase and oxide have exsolved from OPM, then it must be asked what circumstances led to the incorporation of FeTi- and vacancy-bearing (Eskola) components in the original orthopyroxene. Extensive FeTi substitution in pyroxene is well documented in a variety of terrestrial (and lunar) situations, especially in augite phenocrysts that crystallized

rapidly at *low pressure* (*cf.* Tracy & Robinson 1977), although we are unaware of detailed studies of orthopyroxene phenocrysts that bear on this problem.

The few documented examples of an Eskola component in pyroxene are restricted to clinopyroxene at *high pressure*. Smyth (1977) reported ~17% Ca-Eskola component in omphacite from a coesite-bearing mantle xenolith found in South African kimberlite, where he noted the breakdown of this component to $CaAlSiAlO_6 + 3SiO_2$ (as coesite). In experiments on the system $CaO-MgO-Al_2O_3-SiO_2$ at 25–30 kbar, Wood & Henderson (1978) and Gasparik & Lindsley (1980a) produced clinopyroxene with ~20–26 mole % Ca-Eskola component. The effects of iron on these relationships are unknown, nor are there any experimental data for orthopyroxene.

The applicability of these observations and experimental results to OPM is problematic. The pressures implied by the presence of coesite as a breakdown product in the nodule and those recorded in the experiments are far higher than those permitted by the field and petrographic relationships at St-Urbain, where prior and simultaneous crystallization of plagioclase occurred. Moreover, several other compositional characteristics of OPM are not suggestive of a high-pressure origin, including the very low jadeite content of bulk OPM (and associated clinopyroxene) and the high proportion of ^{iv}Al relative to ^{vi}Al.

In light of these problems with a high-pressure origin for OPM, it is appropriate to consider whether other factors are important to the incorporation of vacancy-type components in the orthopyroxene. For example, rapid growth of OPM may lead to the metastable incorporation of such components, and is also a rather effective mechanism for producing high concentrations of Al, Ti, Fe^{3+} and *REE*, since their dissipation at the crystal–melt interface is probably limited by diffusion.

Current models of crystal-growth mechanisms indicate that incorporation of cations into a growing crystal involves initial adsorption onto "protosites" (Nakamura 1973) at the crystal–melt interface. Cations in such protosites may be rejected or retained, depending on factors such as suitability of the crystallographic site and rate of growth. Slow growth allows "undesirable" cations to be desorbed from the crystal surface before (or soon after) the next increment of growth is added, and an equilibrium partitioning is approached. Rapid growth, on the other hand, may not provide sufficient time for desorption to occur. In such a situation, cations with a high charge/radius ratio will tend to be retained selectively, since these adhere more tenaciously to the unsatisfied bonds at the crystal surface (Dowty 1976). Such models have been applied with considerable success to phenomena such as sector zoning in calcic pyroxene, in which the slow-growing (100) sector is enriched in Ti, Al, Fe^{3+} and Na compared to other sectors (*e.g.*, Hollister & Gancarz 1971) because it exposes a higher proportion of *M*1 and *M*2 protosites (Nakamura 1973, Dowty 1976). Shimizu (1981) reported (100)-sector enrichments for a variety of minor and trace elements in sector-zoned augite, and noted that the degree of enrichment correlates with ionic field-strength. This observation appears to confirm the importance of charge/radius ratio in the desorption of cations that were initially adsorbed onto protosites in proportions higher than the equilibrium values for the completed crystallographic sites.

This general model appears to have applicability to the OPM, as the cations that distinguish them from other types of orthopyroxene correspond closely to those cations enriched in (100) sectors of zoned crystals of augite. No data have yet been reported for sector enrichments of *REE* in augite, but charge/radius ratios for the *REE* indicate that they should be preferentially retained in protosites. The enrichment of *REE* in OPM relative to matrix orthopyroxene (Fig. 13) is therefore consistent with and predictable from this hypothesis, although the degree of enrichment (~10×) is significantly greater than that found for other cations with a similar charge/radius ratio; perhaps additional factors, including phase-equilibria controls on the more abundant Al, Ti, Fe^{3+} (*i.e.*, "competition" with cocrystallizing plagioclase and oxide) and charge balancing that must occur as the cations become incorporated in the crystal, have contributed to the observed differences.

For the *REE* themselves, it is noteworthy that the pattern of the OPM from the coarse-grained leuconorite is essentially parallel to that of orthopyroxene in adjacent medium-grained leuconorite. This observation does not lend itself to straightforward interpretation in terms of the adsorption–desorption model discussed above, because the more extensive desorption for the finer-grained (more slowly grown?) orthopyroxene should have resulted in somewhat lower abundances of the light *REE* (lower charge/radius ratio) relative to the heavy *REE* in this material. The parallelism of these patterns strongly suggests that the configuration of the crystallographic site for the *REE* (most likely *M*2) has controlled the relative abundances of the *REE* in both types of orthopyroxene. Only if exposed protosites were sufficiently well defined to discriminate among the *REE* in the same manner as a completed site could the parallelism of the two *REE* patterns be understood in the context of the adsorption–desorption model.

It is interesting that the *REE* patterns of the three OPM in anorthosite have intermediate abundances of *REE* and more strongly fractionated light *REE*

(Fig. 14). These characteristics correspond closely to what would be expected if a crystal–melt interface with *REE* abundances such as those of the OPM in coarse leuconorite had undergone some desorption in attempting to approach the values (presumably closer to equilibrium) in the medium leuconorite orthopyroxene. Such a comparison is highly speculative, however, because we do not yet understand the relationship between the outcrops from which these different materials were obtained.

If an adsorption–desorption model is applicable to the OPM, then some caution is needed concerning the interpretation of Eu anomalies. Eu^{2+} has a lower charge and larger radius than Eu^{3+}; this reduced ionic field-strength indicates that Eu^{2+} is more readily desorbed than Eu^{3+}, which may lead to lower abundances of europium (*i.e.,* larger negative europium anomalies) than expected from equilibrium partition-coefficients and the Eu anomaly of the melt from which the OPM grew. We suspect that the large negative Eu anomalies for OPM principally reflect prior crystallization of plagioclase from the melt because of textural observations, and because the orthopyroxene from the medium-grained leuconorite has only a slightly more negative anomaly ($Eu/Eu^* = 0.38$ *vs.* 0.48 for adjacent OPM). The effect of selective desorption of Eu^{2+} may have contributed to the observed anomalies, however.

An additional factor that may contribute to the origin of OPM compositions is the possibility that they crystallized originally with monoclinic symmetry. If this were the case, then the cation sites in "clinohypersthene" probably could have accommodated higher concentrations of Ca and Al, *etc.,* with plagioclase exsolution occurring during later inversion to the orthorhombic form. However, preliminary single-crystal X-ray photographs of OPM do not show any streaking or other features suggestive of a monoclinic precursor.

In summary, we favor incorporation of Ti, Al, Fe^{3+}, *REE, etc.,* into OPM as a result of rapid crystal-growth in which there was insufficient time for these cations to be rejected (or desorbed) from the crystal surfaces. For this reason, bulk OPM probably do not contain equilibrium abundances of many minor and trace elements. How fast crystals must grow in order for such effects to be important is unclear. If the rate of crystal growth in the anorthosite massif is controlled by heat loss to country rocks, then it is difficult to envision rapid crystal-growth in the plutonic environment of the St-Urbain and other anorthosite massifs. Rather, the spatially restricted occurrence of OPM suggests that their formation was a response to local variations in conditions of crystallization.

One possibility is that the prolonged formation of plagioclase resulted in local overstepping of a plagioclase–orthopyroxene cotectic boundary-curve. Orthopyroxene supersaturation may be permitted by the reluctance of that mineral to nucleate, which is noted in certain experimental studies (*e.g.,* Turnock & Lindsley 1981). Although supersaturation commonly results in the formation of many nuclei, the difficulty in orthopyroxene nucleation may have allowed for the accelerated growth of those few that formed first. The growth of these nuclei would then lead to the formation of isolated occurrences of coarse OPM in which "excess" components (particularly those involving Ca and Al) were incorporated metastably. Eventually, the system returned to cotectic relationships, wherein orthopyroxene with "normal" contents of Ca, Al, Fe^{3+}, Ti and *REE* formed. The peculiar change in facies in leuconorite (Fig. 6) may be an expression of such processes of crystallization. The slightly higher value of Fe/Mg in the *bulk* OPM is consistent with a supersaturation hypothesis, and the metastability of the minor-element components may explain the apparent ease with which they exsolved out of OPM.

This model predicts that OPM should be found in rocks with near-cotectic proportions of plagioclase and pyroxene. The leuconorite that contains OPM (Fig. 6) in fact represents one of the most pyroxene-rich lithologies in the massif, and other occurrences of leuconorite also contain OPM. These observations can be considered as supportive of the supersaturation hypothesis, but the occurrence of OPM in anorthosite is more difficult to explain. However, it is clear from Figure 10 that locally the abundance of OPM is sufficient to describe even these rocks as "leuconorite". The point here is that with the exception of the vein occurrences, OPM have not been identified as isolated single grains, but are always found in clusters of dozens of large crystals.

Implications for characteristics of the parent magma

Probably the most enduring problem surrounding the petrogenesis of massif anorthosites is the nature of their parent magma(s). Various investigators, using numerous approaches and techniques, have proposed magmas ranging from basalt through granodiorite. The principal objection to a basaltic parent-magma as originally formulated by Bowen (1917) is the general absence of rocks rich in mafic minerals that would represent complementary differentiates to the plagioclase-rich rocks of the anorthosite. However, Emslie (1975, 1978) has suggested that OPM are the relics of early crystallization of pyroxene; he developed an intriguing and comprehensive model to link anorthosite to parental olivine basalt magma. Early separation of olivine and pyroxene from an alkali basalt parent-magma forms an integral part of the "reaction melting" model proposed by Barker *et al.* (1975) to account for the

association of some anorthositic rocks with alkali and rapakivi granites. More recently, Morse (1979) has advocated fractionation of olivine + pyroxene during ascent of mafic magma as an effective means of producing highly aluminous Fe-rich liquids parental to anorthosite. The feature that all of these models share is the "burial" of mafic cumulates in the upper mantle (or lower crust). Some of the data presented in this report provide an opportunity to address certain aspects of the parent-magma problem. Specifically, we will examine briefly some mineral-composition and trace-element characteristics of the anorthositic rocks and plausible basaltic analogues.

The compositions of associated plagioclase ($\sim An_{40}$) and orthopyroxene, including OPM ($\sim En_{70}$), are unlike those found in layered mafic intrusive complexes. For example, in the Stillwater complex, cumulus En_{70} orthopyroxene occurs with cumulus $\sim An_{65-70}$ plagioclase (*cf.* Raedecke & McCallum 1980). By comparison, the St-Urbain plagioclase is too Ab-rich, or the orthopyroxene is too Mg-rich, to have crystallized from a similar basaltic melt if both minerals are cumulus phases. A link to a melt of basaltic composition seems even more remote if the St-Urbain orthopyroxene crystallized entirely from interstitial melt between cumulus plagioclase crystals. If sufficient orthopyroxene (± olivine) crystallization had occurred at a prior stage, to produce the highly feldspathic St-Urbain magma from basalt, then it is remarkable that the observed orthopyroxene is so Mg-rich. Perhaps cocrystallization of an oxide like hemoilmenite could perturb these relationships, and future studies should address this possibility. Nevertheless, we consider the difference between the En–An systematics of the St-Urbain body (and many other anorthosites; *cf.* Anderson & Morin 1969) and those in basaltic rocks to be significant.

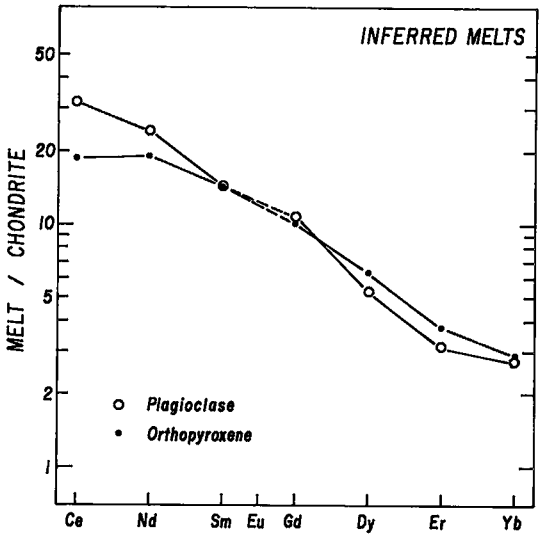

FIG. 22. *REE* patterns of melts calculated to be in equilibrium with purified plagioclase megacryst (Table 4, #7) and orthopyroxene (Table 4, #5) from leuconorite CHV 80–99. Melt patterns are obtained by dividing the mineral *REE* abundances by mineral/melt distribution-coefficients (average of three orthopyroxene distribution-coefficients from Onuma *et al.* (1968) and Schnetzler & Philpotts (1970); plagioclase distribution-coefficients are taken from Drake & Weill (1975). The shape of the *REE* pattern of melts calculated to be in equilibrium with other plagioclase and orthopyroxene in Table 4 are either similar or slightly more fractionated in the heavier *REE*. Eu is not modeled, because of an uncertainty that affects the Eu^{2+}/Eu in melt [T, $f(O_2)$, bulk-composition controls]. The *absolute* values of calculated *REE* abundances of melt are also subject to large uncertainties (factors of 2 to 5), but pattern shapes are tightly constrained. Other possible sources of error include trapped-melt effects and subsolidus equilibration of *REE*, but do not appear significant (*cf.* Gromet & Dymek 1981b).

The exceptionally high contents of Sr in the plagioclase and the somewhat elevated $^{87}Sr/^{86}Sr$ ratios are not features expected for a tholeiitic parent-magma. *REE* patterns of melts calculated to be in equilibrium with plagioclase and orthopyroxene are highly fractionated with steep, monotonic slopes and low concentrations of the heavy *REE* (Fig. 22). These trace-element and isotopic characteristics are generally similar to those observed in a variety of alkalic basalts from continental and oceanic island settings, but there is no geological and petrological evidence to indicate the involvement of such magmas at St-Urbain. In particular, the preponderance of orthopyroxene over calcic pyroxene in the St-Urbain andesine anorthosites and leuconorites is contrary to that expected for an alkali basalt magma.

Although not yet definitive, these geochemical and petrological characteristics of the St-Urbain massif raise some concern regarding a basaltic parent magma. Partial melting of mafic rocks (*e.g.*, Simmons & Hanson 1978) at deep crustal levels under conditions of relatively high $f(O_2)$ provides an attractive alternative. We note that the involvement of garnet-bearing lithologies could help to explain several features of the St-Urbain massif, including the high content of Sr in the plagioclase and its fractionated, heavy-*REE*-depleted patterns, whereas high $f(O_2)$ seems necessary to account for primary magmatic hemoilmenite. We are presently evaluating such mechanisms, and a more complete development of these arguments will be presented in a subsequent paper (Gromet & Dymek, in prep.).

In conclusion, OPM may provide insight into the unusual processes of crystallization occurring dur-

ing the magmatic history of anorthosites, but they are not vestiges of a basaltic parent. Rather than viewing the St-Urbain anorthosite as an orphan of a basalt, we suggest that its source may lie in the deep crust and involve an anorthositic magma, as indicated by the well-developed dykes that we observe in the field.

Acknowledgements

Funding for this work was provided by the U.S. National Science Foundation (grants EAR 80-09223 to Dymek, and EAR 79-11184 and EAR 80-09324 to Gromet). We thank F. Allen and M. Dickensen for carrying out the X-ray and ferrous iron determinations, respectively. Thorough reviews by R.F. Emslie, D.H. Lindsley and A.C. Turnock are most appreciated.

References

Albee, A.L. & Ray, L. (1970): Correction factors for electron probe microanalysis of silicates, oxides, carbonates, phosphates and sulfates. *Anal. Chem.*, **42**, 1408-1414.

Anderson, A.T., Jr. & Morin, M. (1969): Two types of massif anorthosites and their implications regarding the thermal history of the earth. *In* Origin of Anorthosite and Related Rocks (Y.W. Isachsen, ed.). *N.Y. State Mus. Sci. Surv., Mem.* **18**, 57-70.

Barker, F., Wones, D.R., Sharp, W.N. & Desborough, G.A. (1975): The Pikes Peak batholith, Colorado Front Range, and a model for the origin of the gabbro–anorthosite–syenite–potassic granite suite. *Precambrian Res.* **2**, 97-160.

Bence, A.E. & Albee, A.L. (1968): Empirical correction factors for the electron microanalysis of silicates and oxides. *J. Geol.* **76**, 382-403.

Boak, J.L. & Dymek, R.F. (1982): Metamorphism of the ca. 3800 Ma supracrustal rocks at Isua, west Greenland: implications for early Archaean crustal evolution. *Earth Planet. Sci. Lett.* **59**, 155-176.

Bohlen, S.R. & Essene, E.J. (1978): Igneous pyroxenes from metamorphosed anorthosite massifs. *Contr. Mineral. Petrology* **65**, 433-442.

Bowen, N.L. (1917): The problem of the anorthosites. *J. Geol.* **25**, 209-243.

Chambers, W.F. (1978): Sandia - Task '78: an electron microprobe automation program. *Sandia Lab. Res. Rep. SAND* 78-1149.

Dowty, E. (1976): Crystal structure and crystal growth. II. Sector zoning in minerals. *Amer. Mineral.* **61**, 460-469.

Drake, M.J. & Weill, D.F. (1975): Partition of Sr, Ba, Ca, Y, Eu^{2+}, Eu^{3+} and other *REE* between plagioclase feldspar and magmatic liquid: an experimental study. *Geochim. Cosmochim. Acta* **39**, 689-712.

Dymek, R.F. (1980): Petrogenetic relationships between andesine anorthosite dikes and labradorite anorthosite wall rock on Mont du Lac des Cygnes, St. Urbain anorthosite massif, Quebec. *Geol. Soc. Amer. Abstr. Programs* **12**, 419.

Emslie, R.F. (1975): Pyroxene megacrysts from anorthositic rocks: new clues to the sources and evolution of the parent magmas. *Can. Mineral.* **13**, 138-145.

_____ (1978): Anorthosite massifs, rapakivi granites and late Proterozoic rifting of North America. *Precamb. Res.* **7**, 61-98.

Gasparik, T. & Lindsley, D.H. (1980a): Experimental study of pyroxenes in the system $CaMgSi_2O_6$–$CaAl_2SiO_6$–$Ca_{.5}AlSi_2O_6$. *Amer. Geophys. Union Trans.* **61**, 402-403 (abstr.).

_____ & _____ (1980b): Phase equilibria at high pressure of pyroxenes containing monovalent and trivalent ions. *In* Pyroxenes (C.T. Prewitt, ed.). *Mineral. Soc. Amer., Rev. Mineral.* **7**, 309-340.

Gromet, L.P. (1979): *Rare Earth Abundances and Fractionations and their Implications for Batholithic Petrogenesis in the Peninsular Ranges Batholith, California, USA, and Baja California, Mexico.* Ph.D. dissertation, California Institute of Technology, Pasadena, California.

_____ & Dymek, R.F. (1980): Evidence for at least two geochemically distinct anorthosite types in the St. Urbain anorthosite massif, Quebec. *Geol. Soc. Amer. Abstr. Programs* **12**, 438.

_____ & _____ (1981a): Al-rich orthopyroxene megacrysts from the St. Urbain anorthosite massif, Quebec: evidence favoring *in situ* crystallization. *Geol. Soc. Amer. Abstr. Programs* **13**, 464.

_____ & _____ (1981b): Petrological and geochemical characterization of the St. Urbain anorthosite massif, Quebec: summary of initial results. *In* Workshop on Magmatic Processes of Early Planetary Crusts (Extended abstracts, p. 30-32). The Lunar and Planetary Institute, Houston.

Hollister, L.S. & Gancarz, A.J. (1971): Compositional sector-zoning in clinopyroxene from the Narce area, Italy. *Amer. Mineral.* **56**, 959-979.

Martignole, J. & Schrijver, K. (1970): Tectonic setting and evolution of the Morin anorthosite, Grenville Province, Quebec. *Geol. Soc. Finland Bull.* **42**, 165-209.

Masuda, A., Nakamura, N. & Tanaka, T. (1973): Fine structure of mutually normalized rare-earth patterns of chondrites. *Geochim. Cosmochim. Acta* **37**, 239-248.

MAWDSLEY, J.B. (1927): St. Urbain area, Charlevoix District, Quebec. *Geol. Surv. Can. Mem.* **152.**

MORSE, S.A. (1975): Plagioclase lamellae in hypersthene, Tikkoatokhakh Bay, Labrador. *Earth Planet. Sci. Lett.* **26,** 331-336.

_____ (1979): Kiglapait geochemistry. I. Systematics, sampling, and density. *J. Petrology* **20,** 555-590.

NAKAMURA, Y. (1973): Origin of sector-zoning in igneous clinopyroxenes. *Amer. Mineral.* **58,** 986-990.

ONUMA, N., HIGUCHI, H., WAKITA, H. & NAGASAWA, H. (1968): Trace element partition between two pyroxenes and the host lava. *Earth Planet. Sci. Lett.* **5,** 47-51.

POWELL, J.A., GROMET, L.P. & DYMEK, R.F. (1982): Quartz monzodiorites and oxide-apatite-rich norites marginal to the St. Urbain anorthosite massif: products of liquid immiscibility? *Amer. Geophys. Union Trans.* **63,** 456 (abstr.).

POWELL, M.A., WALKER, D. & HAYS, J.R. (1980): Controlled cooling and crystallization of a eucrite: microprobe studies. *Proc. Lunar Planet. Sci. Conf.* **11,** 1153-1168.

RAEDECKE, L.D. & MCCALLUM, I.S. (1980): A comparison of fractionation trends in the lunar crust and the Stillwater complex. *Proc. Conf. Lunar Highlands Crust,* 133-153.

RONDOT, J. (1979): Reconnaissances géologiques dans Charlevoix-Saguenay. *Ministère Richesses Naturelles du Québec DPV-***682.**

ROY, D.W., RONDOT, J. & DYMEK, R.F. (1972): A crypto-explosion structure at Charlevoix and the St. Urbain anorthosite. *Int. Geol. Cong. 24th (Montreal), Guidebook, Excursion B-***06.**

SCHNETZLER, C.C. & PHILPOTTS, J.A. (1970): Partition coefficients of rare-earth elements between igneous matrix material and rock-forming mineral phenocrysts. II. *Geochim. Cosmochim. Acta* **34,** 331-340.

SHIMIZU, N. (1981): Trace element incorporation into growing augite phenocryst. *Nature* **289,** 575-577.

SIMMONS, E.C. & HANSON, G.N. (1978): Geochemistry and origin of massif-type anorthosites. *Contr. Mineral. Petrology* **66,** 119-135.

SMYTH, J.R. (1977): Peraluminous omphacite: cation vacancies in upper mantle pyroxenes. *Amer. Geophys. Union Trans.* **58,** 523 (abstr.).

TRACY, R.J. & ROBINSON, P. (1977): Zoned titanian augite in alkali olivine basalt from Tahiti and the nature of titanium substitutions in augite. *Amer. Mineral.* **62,** 634-645.

TURNOCK, A.C. & LINDSLEY, D.H. (1981): Experimental determination of pyroxene solvi for ≤ 1 kbar at 900 and 1000°C. *Can. Mineral.* **19,** 255-267.

WOOD, B.J. & HENDERSON, C.M.B. (1978): Compositions and unit-cell parameters of synthetic non-stoichiometric tschermakitic clinopyroxenes. *Amer. Mineral.* **63,** 66-72.

Received January 19, 1983, revised manuscript accepted July 19, 1983.

APPENDIX: ANALYTICAL TECHNIQUES

Most of the mineral analyses reported here were carried out on an automated 3-spectrometer ARL EMX-SM microprobe; details of the methods are described in Boak & Dymek (1982). Additional analyses were carried out on a 3-spectrometer CAMECA MBX microprobe equipped with a Tracor-Northern automation system, and interfaced through a DEC PDP-11/04 minicomputer for control and on-line data reduction. Analytical conditions used: accelerating potential 15 kV and beam current of 15 nA, measured directly by means of a Faraday cup. X-ray intensities were converted to weight percent oxides using the methods of Bence & Albee (1968), with correction factors modified from Albee & Ray (1970). Simple silicates and oxides were used as primary standards.

The analysis strategy employed methods modified from those outlined by Chambers (1978). Counting times were adjusted automatically (up to a maximum of 30 seconds), so as to achieve a counting-statistic precision of 1% or better for major elements (about 3 wt.% or greater) and 1–5% for minor elements (~0.5-3 wt.%). Reproducibility of all analyses is judged to be 1–5% of the amount present (depending on concentration) based on repetitive analyses of feldspar and pyroxene internal standards.

Bulk compositions of orthopyroxene megacrysts were determined by microprobe analysis of glass prepared by fusion of equal amounts of sample and $Li_2B_4O_7$. (Sample powders and flux were dried overnight at 110°C; approximately 1 g each was weighed out, carefully mixed, and then fused for ~ 10 minutes at 1100°C in graphite crucibles. The resultant glass bead was crushed in acetone, and then remelted.) Glass analyses were performed by the same general methods as with mineral analyses, except that the stage was translated at the rate of ~ 1 μm/s to minimize possible effects of glass instability under the electron beam.

During initial reduction of data, Li_2O and B_2O_3 were treated as oxides of known concentration. Thereafter, the remaining oxides were normalized to 100% (see Table 6). Analyses of glasses prepared by the same methods from G-2, BCR-1, AGV-1 and W-1 yield results for each oxide within ± 2% (relative) of published values (recalculated to 100%, anhydrous).

Rb-Sr isotopic determinations were performed on a computer-controlled, 12-inch radius-of-curvature, NBS-design mass spectrometer. Samples were dissolved with HF and $HClO_4$. Rb and Sr were separated using standard ion-exchange techniques, and loaded as chlorides onto oxidized double- or single-Ta filaments, respectively. Blanks for chemical processing are 1 ng Sr and 0.05 ng Rb.

REE determinations were performed by isotope-dilution mass spectrometry following methods described in detail by Gromet (1979). Analytical precision is ~ 1–2%. Chondrite-normalized patterns (Figs. 14–16) use the values for the Leedy chondrite (Masuda *et al.* 1973) divided by 1.2.